Integrated Aerodynamic-Structural Design Optimization

by

William M. Eppard

Thesis submitted to the Faculty of the

Virginia Polytechnic Institute and State University

in partial fulfillment of the requirements for the degree of

Master of Science

in

Aerospace Engineering

APPROVED:

B. Grossman, Chairman

R.T. Haftka

J.A. Schetz

June 1987

Blacksburg, Virginia

Integrated Aerodynamic-Structural Design Optimization

by

William M. Eppard

B. Grossman, Chairman

Aerospace Engineering

(ABSTRACT)

The introduction of composite materials in aircraft structures is having a profound effect on the design process. These materials permit the designer to tailor material properties to improve structural and aerodynamic performance. In order to obtain maximum benefits, a more integrated multidisciplinary design process is required. Furthermore, because of the complexity of the combined aerodynamic/structural design process numerical optimization methods are required.

The present research is focused on a major difficulty associated with the multidisciplinary design optimization process - its enormous computational cost. We consider two approaches for reducing this computational burden: (i) development of efficient methods for cross-sensitivity calulation using perturbation methods; and (ii) the use of approximate numerical optimization procedures. Our efforts are concentrated upon combined aerodynamic-structural optimization. Results are presented for the integrated

design of a sailplane wing. The impact of our computational procedures on the computational costs of integrated designs are discussed.

Acknowledgments

I am greatly indebted to Dr. Grossman and Dr. Haftka for their help and guidance in this research. I would also like to thank P.J. Kao who performed the structural/aeroelastic work involved in this project.

This thesis is dedicated to my family, without whose support I would have never have come so far as to actually write this thesis.

TABLE OF CONTENTS

LIST OF TABLES

LIST OF FIGURES

NOMENCLATURE

a_{mn}	Vortex-lattice coefficient for u_{mn}
A	Matrix of C_l sensitivities
A_s	Matrix of Lift sensitivities
b	Span
b_{mn}	Vortex-lattice coefficient for v_{mn}
c_l	Average chord length of ith wing section
$\bar{c}$	Mean chord length
$\overline{C}$	Right-hand-side vector for vortex-lattice system
C_a	Diagonal matrix of chord lengths
C_{D_o}	Parasite drag coefficient
C_D	Total drag coefficient
C_{D_v}	Induced drag coefficient
C_F	Section force coefficient
C_l	Section lift coefficient
$\overline{C}_l$	Lift vector (rigid wing)
$\hat{C}_l$	Lift vector (deformed wing)
C_L	Total lift coefficient

C_m	Element of $\overline{C}$
C_m'	Perturbed element of $\overline{C}$
c_{mn}	Vortex-lattice coefficient for w_{mn}
D	Horizontal distance traveled
$\overline{D}$	Right-hand-side vector for perturbation method
e_i	semiwidth of the ith wing section
E	Force vector transformation matrix
$\overline{F}$	Structural load vector
$\overline{F}_m$	Aerodynamic force on mth panel
g	Gravitational acceleration
$\overline{g}_a$	Aerodynamic constraint
$\overline{g}_s$	Structural constraint
H	Height climbed in thermal
I	Identity matrix
K	Structural stiffness matrix
l_i	Average lift per unit span on ith panel
n	Load factor
n_{dof}	Number of structural degrees of freedom
n_{dv}	Number of design variables
n_p	Number of panels on the starboard wing
n_{p_i}	Number of panels on ith wing section

n_s	Number of spanwise wing sections
$\hat{n}_m$	Unit normal vector to wing mean-camber surface
$\overline{N}$	z-direction vector
q	Dynamic pressure
q_d	Divergence dynamic pressure
R	Turn radius
$\overline{R}$	Incremental C_l vector
$\overline{R}_s$	Incremental force vector
S	Wing planform area
S_f	Reduced flexibility matrix
t	Time
T	Twist tranformation matrix
T_s	Structural transformation matrix
u_{mn}	x-component of $\overline{U}_{mn}$
$\overline{U}$	Vortex induced velocity
$\overline{U}_\infty$	Free-stream velocity vector
v_{mn}	y-component of $\overline{U}_{mn}$
V	Matrix of vortex-lattice influence coefficients
V_{mn}	Component of V
V_{mn}'	Perturbed component of V
V_c	Climb rate in the thermal
V_r	Average cross-country speed

V_{s_1}	Sink speed during climb
V_{s_2}	Sink speed during cruise
V_t	Upward air velocity in the thermal
V_2	Velocity during cruise
w_{mn}	z-component of $\overline{U}_{mn}$
W	Total weight of sailplane
W_S	Diagonal weighting matrix for numerical integration
x,y,z	Cartesian-Coordinate directions for vortex-lattice method
$\overline{x}_a$	Aerodynamic design variable vector
$\overline{x}_s$	Structural design variable vector
x^l	Lower bound on design variable
x^u	Upper bound on design variable
x_j	*j*th design variable
α_b	Base angle-of-attack
α'	Change in angle of attack from α_b
α_{ind}	Induced incidence angle
γ	Coefficient for parabolic function approximating spanwise lift distibution, Eq(2.4.4)
Γ_n	Stength of *n*th vortex
Γ_n'	Perturbed strength of the *n*th vortex
$\overline{\Gamma}$	Vector of vortex strengths
$\overline{\delta}$	Vector of elastic twist angles

	at aerodynamic chords
$\bar{\delta}_s$	Vector of elastic twist angles at structural chords
$\overline{\delta\Gamma}$	Vector change in vorticity
Δy_i	Spanwise width of *i*th wing section
ε	Perturbation angle
η	Spanwise location variable
θ_m	Angle of mean-camber surface with respect to x-axis
θ_p	Flight path angle
λ	Allowable change in jth design variable
ν	Coefficient for parabolic function approximating spanwise lift distribution, Eq(2.4.4)
ρ	Air mass density
φ	Coefficient for parabolic function approximating spanwise lift distribution, Eq(2.4.4)

Chapter 1. Introduction

Aircraft design requires the integration of several disciplines, including aerodynamics, structures, controls, and propulsion. In the traditional design process these disciplines are integrated only during the preliminary design phase, where simple analytical tools are used to make decisions concerning the overall size and shape of the configuration. After this initial design phase, the complexity of the analysis required for each individual-discipline design typically discourages design integration, except in crisis situations. For example, if the wing structural design results in excessive weight, the aerodynamic design may be altered to provide load relief.

This minimal-interaction design process was sufficient for traditional aircraft design, since little could be gained through the increased interaction of disciplines due to the nature of the materials and control systems used. The introduction of composite materials in aircraft design has given rise to situations where significant interdisciplinary (aerodynamic/structural)

interactions occur. Instead of using off-the-shelf materials, it is now possible to custom design material properties to fit the requirements of the product. Materials can be designed to prevent aeroelastic instabilities, to control load distribution or even to improve aerodynamic performance. A case in point is the X-29A forward-swept-wing fighter for which composite materials were tailored to produce favorable aeroelastic-structural interaction. Because a metal forward-swept wing has an inherently destabilizing interaction between bending and twisting, it is not practical to build this type of wing with metal. However, a composite material was tailored to reverse this destabilizing interaction and make the X-29A design possible.

The efficient utilization of tailored materials requires the design integration of several disciplines. For example, consider the three-way interaction between material, structures, and aerodynamics involved in wing design. In order to favorably utilize the interactions between the three disciplines, the design of the wing structure, the material properties, and the aerodynamic shape should proceed in an simultaneous, integrated fashion. However, the materials specialist typically wants to analyze in great detail the micromechanical behavior of the tailored material so as to predict properties and failure characteristics. Similarly, the structural analyst and the aerodynamicist use sophisticated behavioral models which strain the capacity of present-day computers for a single analysis. Integrating such analytical tools in the framework of optimal design, where analyses must be repeated again and

again, presents the major difficulty associated with the multidisciplinary design process - its enormous cost.

Past research, (Refs. [1] and [2]), has focused on clearly establishing the advantages of the integrated design procedure over the more traditional sequential/iterated approach. To do this, we considered the aerodynamic/structural interactions involved in wing design. A simple sailplane wing was chosen as a "test bed" because it is a "two-point" design: optimized circling flight in a thermal followed by efficient cross-country cruise. In addition, the very simple, high aspect-ratio wing allowed the use of very simple analysis methods. Lifting-line theory was used for the aerodynamic loads and beam theory was used to determine the structural deflections. Consistant with this simple model, we used approximately 30 independent design variables to define both the aerodynamic shape (planform and twist) and the composite material structural sizes along with 30-31 aerodynamic, structural, and performance constraints. There were 3 performance design variables including the angle of attack during the turn, the angle of attack during cruise, and the radius of the turn. The design, using numerical optimization procedures, was performed in two manners: A sequential, iterative procedure where the structural and aerodynamic optimizations were performed seperately; and an integrated procedure where the entire design is obtained through a single optimization process. These two procedures are presented schematically in Figs. 1 and 2.

The sequential approach first designed the aerodynamic shape by optimizing the performance (average cross-country speed) using the aerodynamic and performance variables. The optimization was performed for a rigid wing with a given weight and subject to the aerodynamic and performance constraints mentioned earlier. The optimized wing shape was then used for the structural optimization, which minimized wing weight by varying the structural variables, while satisfying the structural constraints. The weight was input to the aerodynamic design, and the process globally iterated until the difference between the weight used for the aerodynamic optimization, and the optimized weight obtained by the structural optimization, dropped below 0.2 percent. To correct for aeroelastic effects, the performance of the final design was optimized by varying only the performance variables, while taking the effects of wing deformations into account.

The second approach was the integrated design procedure, where the aerodynamic and structural designs were performed simultaneously, optimizing a single objective function, either performance or weight. In this procedure all the performance, aerodynamic, and structural design variables may be varied at the same time, allowing changes in the weight and the effects of wing deformations on performance to be accounted for at all times during the optimization process. The integrated design approach is complicated by the need for cross-sensitivity derivatives, which represent the influence of the structure on the aerodynamics and vice-versa. In all cases, the integrated designs achieved a lower weight and improved performance over the iterative,

sequential approach. The integrated designs were characterized by less rigid, higher aspect ratio wings which utilize favorable aerodynamic/structural interactions. This study, as described in Refs. [1] and [2], was performed in order to demonstrate the benefits of integrated design, but did not consider the computational efficiency or practicality of the approach.

The objective of the present work is to investigate the computational costs of multi-disciplinary design. We focus on integrating the processes of aerodynamic and structural designs as a prototype for design integration. Along the lines of a more complete integrated design process, we have replaced the rudimentary analysis tools of lifting-line theory and a simple beam model of the wing structure with more realistic panel methods and a finite-element analysis of the wing structure. These methods will provide for a more exact analysis while allowing more general wing shapes to be considered. However, in order to reduce our computational effort, we utilized simplified aerodynamic and structural models. Namely, a vortex-lattice method with 80-200 panels is used to calculate the aerodynamic loads on the sailplane wing. The finite-element model used 90 nodes and approximately 400 elements. Even these relatively simple methods introduce complexities involving the need for more independent design variables and constraints and are significantly more expensive than the methods used in Ref. [2]. In the present design study, we consider the same structural/aerodynamic design of a sailplane wing which formed the basis of our preliminary design study, to evaluate two methods of reducing the computational costs of integrated

design. These two methods are mentioned briefly below and later discussed in more detail.

As previously mentioned, the interdisciplinary optimization process requires sensitivity information on the influence of design decisions in one discipline on the performance of the other discipline (cross-sensitivities). The calculation of these cross-sensitivity derivatives requires a significant portion of the computational time necessary for a complete optimization. One approach for reducing the computational cost involves the use of efficient methods for cross-sensitivity calculation using perturbation methods. The second approach utilizes approximate optimization procedures to reduce the cost of objective function and constraint evaluation.

In the next section we will discuss the sailplane mission and the development of the performance objective function. We will also discuss in detail the aerodynamic and structural analysis methods used. This is followed by a section on the cross-sensitivity analysis and a section on the design procedure. Finally, we discuss the impact of our computational procedures on the computational costs of the integrated design procedure.

Chapter 2. Analysis Methods

2.1 Sailplane Mission and Performance

The mission profile for the glider involves climbing to a height H in a prescribed thermal, then cruising a distance D while losing the altitude H, as depicted in Fig. 3. In order to differentiate between these two portions of the mission, we use a subscript with values 1 or 2 corresponding to the climb and cruise, respectively. The performance index to be maximized for the mission is the average cross-country speed, which is derived below. Carmichael and Horstmann thermal profiles of various strengths are considered, such as those used in Helwig [3].

The net rate of climb of the sailplane in the thermal is given by

$$V_c(R) = V_t(R) - V_{s_1} \tag{2.1.1}$$

where V_t is the upward velocity of the air at a distance R from the center of the thermal, and V_c is the rate of climb in the thermal. The sink speed in the thermal, V_{s_1} , can be obtained in terms of the lift and drag coefficients during climb C_{L_1} , C_{D_1}, the wing area S, and the total weight W by assuming a small downward flight path angle, θ_p , as

$$V_{s_1} = \frac{C_{D_1}}{C_{L_1}^{1.5}}[1 - (\frac{2W}{\rho S C_{L_1} g R})^2]^{-0.75}(\frac{2W}{\rho S})^{0.5} \qquad (2.1.2)$$

where ρ is the air mass density and g is the gravitational acceleration. This equation is derived in detail in Strauch [1].

The cruise speed is given in terms of the cruise lift coefficient C_{L_2} as

$$V_2 = (\frac{2W}{\rho S C_{L_2}})^{0.5} \qquad (2.1.3)$$

and the sink speed in cruise, V_{s2}, can be obtained in terms of the cruise lift and drag coefficients, C_{L_2} and C_{D_2}, by again assuming a small downward flight path angle as

$$V_{s_2} = \frac{C_{D_2}}{C_{L_2}^{1.5}}(\frac{2W}{\rho S})^{0.5} \qquad (2.1.4)$$

This equation is also derived in Strauch [1].

The cross-country speed is determined from the mission profile as depicted in Fig.3. This speed is defined as

$$V_r = \frac{D}{t} \tag{2.1.5}$$

where t is the total time of travel between points A and C, and D is the horizontal distance from A to C. The gain in height during the spiralling portion of flight is

$$H = t_1 V_c \tag{2.1.6}$$

where t_1 is the time to travel from point A to B in Fig. 3. The loss in height in the cruise portion of flight is

$$H = t_2 V_{s_2} \tag{2.1.7}$$

where t_2 is the time to travel from point B to C in Fig. 3. By equating the height gained in the climb to the that lost in the cruise portion we obtain

$$t_1 = t_2 \frac{V_{s_2}}{V_c} \tag{2.1.8}$$

And, knowing that

$$t_2 = \frac{D}{V_2 \cos \theta_p} \tag{2.1.9}$$

and

$$t = t_1 + t_2 \tag{2.1.10}$$

results in

$$t = \frac{D}{V_2 \cos \theta_p}\left(1 + \frac{V_{s_2}}{V_c}\right) \tag{2.1.11}$$

Again assuming a small flight path angle, θ_p, the cross-country speed is found to be

$$V_r = \frac{V_2 V_c}{V_c + V_{s_2}} \tag{2.1.12}$$

The average cross-country speed V_r serves as the performance index for the design study.

2.2 Vortex-Lattice Method

The aerodynamic loads are found using a vortex-lattice method (VLM), such as discussed in Bertin and Smith [4]. In this approach, the continuous distribution of bound vorticity over the wing surface is approximated by a finite number of discrete horseshoe vortices that are placed in trapezoidal panels, as shown in Fig. 4. The bound vortices coincide with the quarter-chord of each panel and are located on the mean camber surface of the wing. It is assumed that the trailing vortices leave the wing and extend downstream to infinity, parallel to the x-axis. This orientation of the trailing vortices simplifies the

calculation of the influences of the vortices (influence coefficients), and causes these coefficients to be independent of angle-of-attack. A more rigorous method would allow the wake to be modeled as a stream surface having zero pressure loading imposed by the surrounding flow. The control point of each panel also lies on the mean camber surface of the wing. It is centered in the spanwise direction between the two trailing vortex legs and lies on the three-quarter-chord line of the panel as shown in Fig. 4.

Because the flow field under consideration is symmetric with respect to the y=0 plane, (i.e., there is no yaw), the lift force acting at a point on the starboard wing (+y) is equal to that at the corresponding point on the port wing (-y). Thus, we need only to solve for the vortex strengths of the starboard wing. To do this, we apply the flow tangency boundary condition on the mean camber surface at each of the control points on the starboard wing, while including the contributions of the horseshoe vortices on the port wing to the velocities induced at these control points. This yields a set of n_p simultaneous equations in the unknown vortex circulation strengths (n_p is the number of panels on the starboard wing).

The velocity induced at some point in space C, a distance r away from a vortex filament of strength Γ_n and length dl is given by the Biot-Savart Law as

$$d\bar{U} = \frac{\Gamma_n(d\bar{l} \times \bar{r})}{4\pi r^3} \qquad (2.2.1)$$

If we consider a straight-line vortex segment AB with vorticity directed from A to B, where $\bar{r}_o$, $\bar{r}_1$, and $\bar{r}_2$ designate the vectors $\overline{AB}$, $\overline{AC}$, and $\overline{BC}$ respectively as shown in Fig. 5, we can integrate the Biot-Savart relation along the length of the vortex filament (from A to B) to obtain an expression for the magnitude of the induced velocity at point C. The result, which is given below, forms the basis for calculating the induced velocity resulting from the horseshoe vortices in the VLM and is derived in detail in Bertin and Smith [4].

$$\overline{U} = \frac{\Gamma_n}{4\pi} \frac{\bar{r}_1 \times \bar{r}_2}{|\bar{r}_1 \times \bar{r}_2|} [\bar{r}_o (\frac{\bar{r}_1}{|\bar{r}_1|} - \frac{\bar{r}_2}{|\bar{r}_2|})] \tag{2.2.2}$$

Consider now the horseshoe vortex shown in Fig. 6., that is representative of the vortex system for a typical wing panel. The bound-vortex portion of the horseshoe vortex is represented by the segment AB, and coincides with the quarter-chord line of the panel. The points A and B lie on the mean-camber surface of the wing and the trailing vortices extend from A to infinity and B to infinity parallel to the x-axis. The resultant induced-velocity vector at some point C is calculated by considering separately the influence of each of the three elements of the vortex system; the bound portion from A to B and each of the two trailing vortex filaments. The resultant velocity vector induced at the *m*th control point by the vortex system on the *n*th panel, $\overline{U}_{mn}$, is represented by

$$\overline{U}_{mn} = u_{mn}\hat{i} + v_{mn}\hat{j} + w_{mn}\hat{k} \tag{2.2.3}$$

where

$$u_{mn} = a_{mn}\,\Gamma_n \tag{2.2.4a}$$

$$v_{mn} = b_{mn}\,\Gamma_n \tag{2.2.4b}$$

$$w_{mn} = c_{mn}\,\Gamma_n \tag{2.2.4c}$$

The equations for the coefficients a_{mn}, b_{mn}, and c_{mn} are derived in Bertin and Smith [4], and depend only on the location of the two vortex corner points and control point under consideration. In combining the above relations, the induced-velocity vector may be written as

$$\overline{U}_{mn} = (a_{mn}\,\hat{i} + b_{mn}\,\hat{j} + c_{mn}\,\hat{k})\Gamma_n \tag{2.2.5}$$

Because the governing equation is linear, the total velocity induced at the mth control point is the summation of the velocities induced by each of the horseshoe-vortex systems.

$$\overline{U}_m = \sum_{n=1}^{2n_p} (a_{mn}\,\hat{i} + b_{mn}\,\hat{j} + c_{mn}\,\hat{k})\Gamma_n \tag{2.2.6}$$

It is noted that $2n_p$ results from the mirror image of the n th horseshoe vortex on the starboard wing. We may rewrite the above equation as

$$\overline{U}_m = \sum_{n=1}^{n_p} [(a_{mn_s} + a_{mn_p})\hat{i} + (b_{mn_s} + b_{mn_p})\hat{j} + (c_{mn_s} + c_{mn_p})\hat{k}]\Gamma_n \tag{2.2.7}$$

where the subscripts s and p stand for the influence of the *n*th horseshoe vortex located on the starboard wing and its mirror image located on the port wing respectively.

As previously stated, we need only apply the flow-tangency boundary condition at each of the control points on the starboard wing. At the *m*th control point we must satisfy

$$\overline{U}_m \cdot \hat{n}_m + \overline{U}_\infty \cdot \hat{n}_m = 0 \tag{2.2.8}$$

where $\overline{U}_\infty$ is the free-stream velocity vector.

$$\overline{U}_\infty = \cos\alpha\, \hat{i} + \sin\alpha\, \hat{k} \tag{2.2.9}$$

The quantity $\hat{n}_m$ is the unit vector normal to the wing mean-camber surface at the *m*th control point given as

$$\hat{n}_m = -\sin\theta_m\, \hat{i} + \cos\theta_m\, \hat{k} \tag{2.2.10}$$

for a wing with no dihedral. The angle θ_m is defined as the angle between the mean-camber surface and the x-axis at the *m*th control point. The boundary condition at the *m*th control point may now be written as

$$\sum_{n=1}^{n_p} [-(a_{mn_s} + a_{mn_p}) \sin\theta_m + (c_{mn_s} + c_{mn_p}) \cos\theta_m]\Gamma_n = \tag{2.2.11}$$

$$\cos\alpha \sin\theta_m - \sin\alpha \cos\theta_m$$

Application of this equation at each of the n_p control points yields a system of n_p simultaneous equations in the unknown vortex strengths, Γ_n , given by

$$V\overline{\Gamma} = \overline{C} \tag{2.2.12}$$

where V is the matrix of influence coefficients, whose elements V_{mn} , represent the normal velocity induced at the mth control point by the vortex on the nth panel. The vector $\overline{C}$ represents the normal component of the free-stream velocity at each control point. These quantities are given by:

$$V_{mn} = -(a_{mn_s} + a_{mn_p}) \sin\theta_m + (c_{mn_s} + c_{mn_p}) \cos\theta_m \tag{2.2.13a}$$

$$C_m = \cos\alpha \sin\theta_m - \sin\alpha \cos\theta_m \tag{2.2.13b}$$

Once the vortex circulations have been obtained, the total-velocity vector, $\overline{U}_{\gamma m}$, (including the free-stream contribution), resulting at the midpoint of each bound vortex can be determined. The force on each panel is then determined by applying the Kutta-Joukowski theorem to the vortex bound to that panel. That is, the force per unit span on the mth panel is

$$\overline{F}_m = \rho \overline{U}_{\gamma m} \times \overline{\Gamma}_m \tag{2.2.14}$$

where $\overline{\Gamma}_m$ is the directed vortex strength of the mth panel; it is Γ_m times a unit vector in the direction of the bound vortex. The total force per unit span resulting on the ith wing section (see Fig. 7) is obtained by summing the contribution from each panel within that chordwise strip. These forces are

then transformed to section force coefficients in the x and z directions as follows

$$(C_{F_x})_i = \frac{\sum_{m=1}^{n_{p_i}} F_{m_x}}{.5\rho U_\infty^2 c_i} \tag{2.2.15a}$$

and

$$(C_{F_z})_i = \frac{\sum_{m=1}^{n_{p_i}} F_{m_z}}{.5\rho U_\infty^2 c_i} \tag{2.2.15b}$$

where U_∞ is the magnitude of the free-stream velocity, (which has been nondimensionalized to one), c_i is the value of the chord length at the spanwise midpoint of the ith wing section and n_{p_i} is the number of panels on the ith wing section. The section lift coefficient for each wing section is then given by the transformation

$$C_{l_i} = - C_{F_{x_i}} \sin\alpha + C_{F_{z_i}} \cos\alpha \tag{2.2.16}$$

where α is the angle of attack.

2.3 Lift

Since the flow is symmetrical, the total lift for the wing is

$$L = 2\int_0^{\frac{b}{2}} l\, dy \tag{2.3.1}$$

where b is the span and l is the lift per unit span. Partitioning the starboard wing into an infinite number of spanwise sections, we obtain

$$L = 2 \lim_{\Delta y_i \to 0} \Sigma_i\, l_i\, \Delta y_i \tag{2.3.2}$$

where l_i is the average lift per unit span on panel i and Δy_i is the width of panel i (see Fig. 7). Introducing the definitions for the section lift coefficient and total lift coefficient we obtain

$$C_L = \frac{2}{S} \lim_{\Delta y_i \to 0} \Sigma_i\, C_{l_i}\, c_i\, \Delta y_i \tag{2.3.3}$$

Here C_{l_i} is the average lift coefficient of panel i, c_i is the average chord for panel i, and S is the total wing area. Once a solution for the section lift coefficient has been obtained, the total lift coefficient may be approximated in terms of a finite number of wing sections as

$$C_L = \frac{2}{S} \sum_{i=1}^{n_s} C_{l_i}\, c_i\, \Delta y_i \tag{2.3.4}$$

where n_s is the number of spanwise sections.

2.4 Vortex Induced Drag

Again, once the solution for the section lift coefficient has been obtained we may write the induced drag coefficient, following Multhopp [5], as

$$C_{D_v} = \frac{2}{S}\int_0^{\frac{b}{2}} C_l\, c\, \alpha_{ind}\, dy \tag{2.4.1}$$

where α_{ind}, the induced incidence, is given by

$$\alpha_{ind} = -\frac{1}{8\pi}\int_0^{\frac{b}{2}} \left[\frac{C_l\, c}{(y-\eta)^2} + \frac{C_l\, c}{(y+\eta)^2}\right] d\eta \tag{2.4.2}$$

for a wing with symmetrical loading. It is noted that η is the spanwise location variable and y is the fixed spanwise location where the induced incidence is to be calculated. Following the approach of Kalman *et al.* [6], we consider the ith wing section having a semiwidth of e_i ,$(e_i = \frac{\Delta y_i}{2})$, and whose centerline is located at $\eta = y_i$ as shown in Fig. 7. Also note that

$$y_{i+1} = y_i + (e_i + e_{i+1}) \tag{2.4.3a}$$

$$y_{i-1} = y_i - (e_i + e_{i-1}) \tag{2.4.3b}$$

We now approximate the spanwise lift distribution across the i th wing section by a parabolic function as:

$$\left(\frac{C_l\, c}{C_L\, \overline{c}}\right)_i = \gamma_{1_i}\eta^2 + \varphi_{1_i}\eta + \nu_{1_i} \tag{2.4.4}$$

where $\bar{c}$ is the mean chord for the wing. From the known solution for the section lift coefficient, we may solve for the coefficients γ_{1_i}, φ_{1_i} , and ν_{1_i} to obtain

$$\nu_{1_i} = (\frac{C_l c}{C_L \bar{c}})_i - \gamma_{1_i}\eta_i^2 + \varphi_{1_i}\eta_i \tag{2.4.5a}$$

$$\gamma_{1_i} = \frac{1}{d_{1_i}d_{2_i}(d_{1_i} + d_{2_i})}\{d_{1_i}(\frac{C_l c}{C_L \bar{c}})_{i+1} - (d_{1_i} + d_{2_i})(\frac{C_l c}{C_L \bar{c}})_i + d_{2_i}(\frac{C_l c}{C_L \bar{c}})_{i-1}\} \tag{2.4.5b}$$

and

$$\varphi_{1_i} = \frac{1}{d_{1_i}d_{2_i}(d_{1_i} + d_{2_i})}\{d_{2_i}(2\eta_i - d_{2_i})[(\frac{C_l c}{C_L \bar{c}})_i - (\frac{C_l c}{C_L \bar{c}})_{i-1}] \tag{2.4.5c}$$

$$- d_{1_i}(2\eta_i - d_{1_i})[(\frac{C_l c}{C_L \bar{c}})_{i+1} - (\frac{C_l c}{C_L \bar{c}})_i]\}$$

where

$$d_{1_i} = e_i + e_{i-1} \tag{2.4.6a}$$

and

$$d_{2_i} = e_i + e_{i+1} \tag{2.4.6b}$$

At the root, for a symmetrical load distribution we have

$$\left(\frac{C_l c}{C_L \bar{c}}\right)_{i-1} = \left(\frac{C_l c}{C_L \bar{c}}\right)_i \tag{2.4.7a}$$

and

$$e_{i-1} = e_i \tag{2.4.7b}$$

At the tip, we take

$$\left(\frac{C_l c}{C_L \bar{c}}\right)_{i+1} = 0 \tag{2.4.8a}$$

and

$$e_{i+1} = 0 \tag{2.4.8b}$$

Substituting these relations into the parabolic function for the spanwise lift distribution, Eq(2.4.4), and then substituting into the equation for the induced drag, Eq(2.4.2), and integrating we obtain

$$\frac{\alpha_{ind}(y)}{C_L \bar{c}} = -\frac{1}{4\pi} \sum_{i=1}^{n_s} \{ \frac{y^2(y_i + e_i)\gamma_{1_i} + y^2 \varphi_{1_i} + (y_i + e_i)\nu_{1_i}}{y^2 - (y_i + e_i)^2} \tag{2.4.9}$$

$$- \frac{y^2(y_i - e_i)\gamma_{1_i} + y^2 \varphi_{i_1} + (y_i - e_i)\nu_i}{y^2 - (y_i - e_i)^2}$$

$$+ \frac{1}{2} y \gamma_{1_i} \log \frac{[(y - e_i)^2 - y_i^2}{(y + e_i)^2 - y_i^2}]^2$$

$$+ \frac{1}{4}\varphi_{1_i} \log\left[\frac{y^2 - (y_i + e_i)^2}{y^2 - (y_i - e_i)^2}\right]^2 + 2e_i\gamma_{1_i}\}$$

We now assume that the product $C_l c\alpha_{ind}$ also has a parabolic variation across the section and write at the i th section

$$\left[\left(\frac{C_l c}{C_L \bar{c}}\right)\left(\frac{\alpha_{ind}}{C_L \bar{c}}\right)\right]_i = \gamma_{2_i} y^2 + \varphi_{2_i} y + \nu_i \tag{2.4.10}$$

The coefficients γ_{2_i}, φ_{2_i} , ν_{2_i} are obtained in an approach identical to that used to find γ_{1_i}, φ_{1_i} , and ν_{1_i}. The numerical form for the induced drag coefficient is given by:

$$\frac{C_{D_v}}{C_L^2} = \frac{4}{AR} \sum_{i=1}^{n_s} e_i \{ [y_i^2 + (\frac{1}{3})e_i^2] \gamma_{2_i} + y_i \varphi_{2_i} + \nu_{2_i}\} \tag{2.4.11}$$

2.5 Profile Drag

In the present design study, the airfoil section is a constant at all spanwise locations (the Boeing BoAR-80-RPVT-16B). The airfoil shape and $C_l - C_d$ curve are shown in Fig. 8. The profile drag coefficient at each wing section is obtained by using the section lift coefficient at that point and the $C_l - C_d$ curve for this airfoil section. The profile drag coefficient is assumed to be constant over the wing section and the total profile drag coefficient is found

by summing each local profile drag coefficient multiplied by the respective section area and then dividing by the total wing area.

The parasitic drag coefficient resulting from the fuselage and tail is treated as a function of wing area as in Helwig [3],

$$C_{D_0} = \frac{constant}{S} \tag{2.5.1}$$

where the constant depends on the type of aircraft. For the sailplane discussed here, a value of .08 was used.

2.6 Finite-Element Method

The structural details of the wing are shown in Fig. 9. The skin and the spar webs are of a sandwich construction of Kevlar face sheets with a foam core. The main spar is an I-beam with spar caps built of unidirectional graphite fibers oriented spanwise. The structural analysis was performed using a modified version of the finite element program WIDOWAC [7]. Eight aerodynamic chords are used for the placement of the aerodynamic loads. Fig. 10 shows their locations along the wing span and the grid points used for a typical cross-section. The aerodynamic loads are applied at the aerodynamic center of each cross-section, namely grid point 7. The model has 90 nodes and 409 elements. We use 192 anisotropic quadrilateral membrane elements to model the skins, which are stacked with 0^o, $+45^o$, -45^o , and

90° plies. Seventy-six shear web elements model the spar webs. The remaining elements are the bar elements which model the spar caps and the vertical stiffness of the ribs and spar webs. Maximum strain constraints ($\varepsilon_1, \varepsilon_2, \varepsilon_{12} < 0.004$) were imposed on each composite lamina. For the spar caps, the strain is limited to 0.003. Tsai-Hill criterion is used for the shear stresses in the spar webs with a shear strength of 6000 $\frac{N}{cm^2}$. Finally, the total weight of the sailplane is calculated with the fuselage and tail section weight assumed to be a constant 130 kg.

2.7 Aeroelastic Analysis

In the present study, it is assumed that for a high-aspect-ratio wing, only torsional deformations have significant aeroelastic effects. The present aeroelastic analysis includes only the effect of torsional deformations on the lift distribution and neglects the change in moment due to torsional deformations and the effects of vertical displacements.

The load vector $\bar{F}$ (of order n_{dof}), corresponding to the structural grid, depends on the vehicle angle of attack α , and the vector of elastic twist angles, $\bar{\delta}_s$ (of order n_s) corresponding to the structural chords: We may write $\bar{F}$ as

$$\bar{F} = \bar{F}_b + E\,(\alpha'\, q\, \bar{R}_s + q\, A_s\, \bar{\delta}_s) \tag{2.7.1}$$

where $\bar{F}_b$ is the force vector of order n_{dof} corresponding to the undeformed structure at some initial angle of attack α_b, α' is the change in angle of attack

from α_b, $\bar{R}_s$ is the incremental force vector (of order n_s) per unit change in angle of attack from α_b, q is the dynamic pressure, and A_s is a n_s by n_s matrix corresponding to the structural chords, such that $qA_{s_{ij}}$ represents the change in lift force at chord i due to a unit twist angle at chord j. The elements of the $\bar{R}_s$ vector are the sum of the corresponding rows of A_s and E is a n_{dof} by n_s matrix that transforms force vectors from the aerodynamic centers to the structural grid. The quantity n_{dof} is the number of degrees of freedom for the structural model and n_s is the number of spanwise stations used in both the structural and aerodynamic models. It is noted that the spanwise locations of the aerodynamic and structural stations need not correspond, and the twist angles at the aerodynamic chords, $\bar{\delta}$, are related to those at the structural chords by

$$\bar{\delta} = T_s^t \bar{\delta}_s \tag{2.7.2}$$

The matrix A_s is obtained from

$$A_S = T_S W_S C_a A T_s^t \tag{2.7.3}$$

where T_s is the transformation matrix relating quantities at the aerodynamic chords to quantities at the structural chords, C_a is a diagonal matrix of aerodynamic chord lengths, and W_s is a diagonal weighting matrix for numerical integration. The matrix A correspondes to the aerodynamic chords, and its elements, A_{ij} , represent the change in lift coefficient at chord *i* due to

a unit twist angle at chord j. The development of the A matrix is described in detail in the following section.

The twist vector $\bar{\delta}_s$ due to $\bar{F}$ is given as

$$\bar{\delta}_s = S_f(\alpha' q \bar{R}_s + q A_s \bar{\delta}_s) + TK^{-1}\bar{F}_b \tag{2.7.4}$$

where S_f is a reduced flexibility matrix relating forces at the aerodynamic centers of the n_s chords to the twist angles at these chords. The matrix T relates displacements of the structural grid to twist angles, and K is the structural stiffness matrix. The S_f matrix was obtained by applying a unit load at the n_s stations, calculating the displacement field, and evaluating the twist from the vertical displacements of the leading edge and trailing edge at each chord. We also have as a requirement that the total force on one wing is equal to half the weight W of the aircraft times the load factor n

$$\bar{N}^t E(\alpha' q \bar{R}_s + q A_s \bar{\delta}_s) + \bar{N}^t \bar{F}_b = \frac{1}{2} nW \tag{2.7.5}$$

where $\bar{N}$ is a vector of order n_{dof} with all components in z direction equal to 1. Using the above equation, we obtain for the corresponding change in angle of attack

$$\alpha' = \frac{(0.5\, n\, W - q\, \bar{N}^t\, E\, A_s\, \bar{\delta}_s - \bar{N}^t\, \bar{F}_b)}{q\, \bar{N}^t\, E\, \bar{R}_s} \tag{2.7.6}$$

Substituting this result into the relation for $\bar{\delta}_s$, Eq(2.7.4), yields

$$\bar{\delta}_s = S_f(\beta\, q\, \bar{R}_s + q\, A_s^* \bar{\delta}_s) + T K^{-1} \bar{F}_b \tag{2.7.7}$$

where

$$A_s^* = A_s - \frac{(\bar{R}_s \bar{N}^t E\, A_s \bar{\delta}_s - \bar{N}^t \bar{F}_b)}{\bar{N}^t E\, \bar{R}_s} \tag{2.7.8}$$

and

$$\beta = \frac{(0.5\, n\, W - \bar{N}^t \bar{F}_b)}{q\, \bar{N}^t E\, \bar{R}_s} \tag{2.7.9}$$

Finally, we get

$$(I - q\, S_f A_s^*)\bar{\delta}_s = \beta\, q\, S_f \bar{R}_s + T K^{-1} \bar{F}_b \tag{2.7.10}$$

where I is the identity matrix. $\bar{\delta}_s$ is now obtained by solving Eq(2.7.10).

The divergence dynamic pressure is obtained by solving the eigenvalue equation

$$(I - q\, S_f A_s)\bar{\delta}_s = 0 \tag{2.7.11}$$

with the lowest eigenvalue corresponding to the divergence dynamic pressure, q_d. In this case we use A_s instead of A_s^* because the former includes the effect of a pilot correction to angle-of-attack to keep the lift force constant. During divergence, the pilot has no time to apply this correction.

Chapter 3. Cross-Sensitivity Analysis

3.1 Approximate Cross-Sensitivity Derivatives

The integrated design approach is characterized by the need for cross-sensitivity derivatives, which allow the integrated design to account for aeroelastic effects that may be controlled for improving aerodynamic performance or redistributing aerodynamic loads. The key step in reducing the cost of cross-sensitivity derivatives is to characterize the interaction between the structural and aerodynamic response by a small number of parameters. In the present study this is affected by assuming that for a high-aspect-ratio wing, only torsional deformations have significant aeroelastic effects. Consistant with this, the aeroelastic analysis, as previously described, involves only the effect of torsional deformations on the lift distribution. Thus, it is enough to calculate a matrix A of sensitivities A_{ij} which represent the change in lift coefficient at chord i due to a unit twist at chord j. A new vector

of total lift distribution is then given in terms of the vehicle angle of attack, a vector of local twist angles $\bar{\delta}$ and the base lift distribution $\bar{C}_{l_b}$ as

$$\bar{C}_l = \bar{C}_{l_b} + \alpha' \bar{R} + A\,\bar{\delta} \tag{3.1.1}$$

where α' is the change in vehicle angle of attack from α_b, (α_b is the vehicle angle of attack corresponding to the base lift distribution), and $\bar{\delta}$ is the vector of torsional deformations corresponding to the aerodynamic chords. The vector $\bar{R}$ represents the incremental change in section lift coefficient per unit change in angle of attack from α_b and its elements are the sum of the corresponding rows of A.

3.2 Analytical Calculation of the A Matrix

The A matrix is found for a given wing planform and twist distribution using the vortex-lattice method and unit displacement states as follows. First, the base lift distribution is determined by a VLM analysis for some median angle-of-attack. Next, a unit rotation is imposed at the first wing section and a new lift distribution is found from a second VLM analysis. The difference between the new lift coefficients and the base lift coefficients at each of the stations forms the first column in the A matrix. The other columns are found in a similar manner.

As previously described, the vortex-lattice method uses a finite number of horseshoe vortices to approximate the continous distribution of bound

vorticity over the wing surface. The application of the flow-tangency boundary condition on the mean-camber surface of the wing yields an n_p by n_p system, (n_p being the number of panels) in the unknown vortex strengths Γ_n as given in Eq(2.2.12) where V is the matrix of influence coefficients, which represent the normal velocity induced at the control points and the vector $\overline{C}$ represents the normal component of free-stream velocity at each control point. The development of the A matrix requires that we set up and solve a system of this type n_s+1 times, where n_s is the number of spanwise wing stations. This represents a significant portion of the total computational time necessary for the complete design cycle.

3.3 Approximate A Matrix Calculation

In order to reduce the costs associated with the A matrix computation we have developed an approximate form of the vortex-lattice method based on small perturbations. However, this linearized vortex-lattice solution will provide an exact result for the derivative of C_l with respect to twist angle at the baseline values of C_l and twist, which corresponds to the A matrix. Let the system of Eq(2.2.12) represent the vortex-lattice solution for a wing in its initial state. If we consider a perturbation where the *i*th spanwise wing section is rotated from its initial state through a small twist angle ε , we obtain the perturbed system

$$V'\overline{\Gamma}' = \overline{C}' \tag{3.3.1}$$

where

$$V'_{mn} = V_{mn} + \varepsilon \delta V_{mn} \tag{3.3.2a}$$

$$\Gamma'_n = \Gamma_n + \varepsilon \delta \Gamma_n \tag{3.3.2b}$$

$$C'_m = C_m + \varepsilon \delta C_m \tag{3.3.2c}$$

If we consider the equation at the mth control point for the perturbed state, we obtain

$$V'_{m1}\Gamma'_1 + V'_{m2}\Gamma'_2 + \ldots + V'_{mn}\Gamma'_n + \ldots + V'_{mn_p-1}\Gamma'_{n_p-1} \tag{3.3.3}$$

$$+ V'_{mn_p}\Gamma'_{n_p} = C_m'$$

Substituting the relations for V_{mn}' , Γ_{mn}' , and C_{mn}' into the above equation and noting that the initial vorticity distribution satisfies $V\overline{\Gamma} = \overline{C}$ and neglecting the terms $o(\varepsilon^2)$ yields

$$V\overline{\delta\Gamma} = \overline{D} \tag{3.3.4}$$

where V is the constant matrix of influence coefficients corresponding to the base lift distribution and $\overline{\delta\Gamma}$ is the vector change in vorticity. The right hand side is the vector $\overline{D}$ whose elements are given by

$$D_m = \delta C_m - \sum_{n=1}^{n_p} \Gamma_n \delta V_{mn} \tag{3.3.5}$$

and the δC and δV terms are found readily from geometry.

The development of the A matrix using this approach requires one VLM analysis to obtain the initial influence matrix V, the initial vorticity distribution Γ, and the initial vector lift distribution $\overline{C}_{l_b}$. It also requires that we set up and solve a system of the type $V\overline{\delta\Gamma} = \overline{D}$ n_s times (i.e., once for each wing section). The major advantage of this approach is that the identical influence matrix for the base lift distribution, V, is used in each solution for $\overline{\delta\Gamma}$. The L-U decomposition of V may be stored and reutilized in the evaluation of the A matrix. This significantly reduces the computational cost. We quantify the savings by considering a single design cycle and examine the computational time on an IBM 3090 for a wing with between 80 and 200 vortex panels. Tables 1 and 2 give the computational time breakdown in the development of the A matrix using the exact vortex-lattice method and the perturbation method respectively for 80 and 120 panels. It is noted that for this study, the number of spanwise stations increased linearly with the number of panels. We see that an overall savings of 20.7 percent occurs for the 80 panel case along with a 34.3 percent savings for the 120 panel case. The overall CPU times for an A matrix evaluation with 80-200 panels is shown in Table 3.

Chapter 4. Design Procedures

4.1 Variables and Constraints

The design variables and constraints used in the present study are given in Tables 4 and 5. The wing planform is described by variable chord lengths at the root, tip, and break (a point between the tip and root) and a variable distance to this break. The chord lengths vary linearly from root to break and from break to tip. The geometric twist is defined by variables at the break and the tip and also varies linearly from root to break and from break to tip. The planform is shown in Fig. 11. Three performance design variables are considered, including the vehicle angle of attack during the turning maneuver and during the cruise portion of the flight, along with the radius of the turn. The structural design variables consist of the spar cap thicknesses, spar web thicknesses, and skin thicknesses at each wing section (see Fig. 9). The aerodynamic constraints consisted of a maximum bank angle, a minimum climb speed, and no stall at any wing section. The stall condition was checked

by making sure that none of the local section lift coefficients exceeded the two-dimensional section stall value of 1.4. The structural constraints are imposed at a design point for a 5.9g pull-up maneuver with a maximum speed of 43 m/s. These constraints included stresses in the spar webs and the skin, strains in the spar caps and skin, and a minimum divergence speed.

4.2 Numerical Optimization Procedure

In the integrated design procedure the aerodynamic and structural designs are performed simultaneously by optimizing a single objective function; in this case maximizing the average cross-country speed. The program used for the numerical optimization process is NEWSUMT-A. A detailed description of the program is given in references [8] and [9]. The basic algorithm is a sequence of unconstrained minimizations using penalty functions to account for constraints and Newton's method with approximate derivatives for unconstrained minimizations.

For the sailplane design study, the optimization problem may be formulated as

$$\textit{maximize} \quad V_r(\bar{x}_a, \bar{x}_s) \tag{4.2.1}$$

$$\textit{such that} \quad g_a(\bar{x}_a, \bar{x}_s) \geq 0 \tag{4.2.2a}$$

$$\textit{and} \quad g_s(\bar{x}_a, \bar{x}_s) \geq 0 \tag{4.2.2b}$$

and the side bounds on the design variables

$$x_a^l \leq x_a \leq x_a^u \tag{4.2.3a}$$

$$x_s^l \leq x_s \leq x_s^u \tag{4.2.3b}$$

where V_r represents the objective function (performance), g_a represents the aerodynamic design constraints, and g_s represents the structural constraints. The vectors $\bar{x}_a$ and $\bar{x}_s$ represent the aerodynamic and structural design variables respectively. NEWSUMT-A systematically modifies some initial design vector while generating a sequence of vectors so that V_r increases or the degree of constraint satisfaction is improved. This sequence of vectors converges to a solution $(\vec{x}_a, \vec{x}_s)$ where the constraint violation is very small and V_r $(\vec{x}_a, \vec{x}_s)$ is at least a local minimum.

4.3 Approximate Optimization Procedure

When the calculations of the objective function and constraints are expensive, it is not feasible to optimize directly the design problem by connecting the optimization algorithm with the analysis codes. Instead, a sequential approximate optimization algorithm is considered to be the best approach [10]. This approach replaces the original objective function and constraints with approximations based upon nominal values and derivatives at an initial point. Move limits are used to prevent the design from moving outside the bound of validity of the approximations. After an optimum is found, a new

approximation is constructed there, and the process repeated until convergence is achieved.

When we first attempted to use the sequential approximate optimization for the combined structural/aerodynamic problem, convergence was found to require extremely tight move limits of one or two percent change in design variables. The problem was traced to the objective function, the average cross-country speed of the glider V_r, which cannot be adequately represented by a linear approximation near the optimum, where it is quite flat. This problem was solved by using a linear approximation to the elements of the A matrix and to the lift distribution on the wing (including the effects of structural deformations) and calculating the performance exactly, from the approximate lift distribution. It was found that the lift distribution is represented well by the linear approximation, so that large changes in the design variables became possible at each approximate optimization. Each approximate optimization problem starting from an initial design $\bar{x}_a^o$, $\bar{x}_s^o$ is formulated as

$$\textit{maximize} \quad V_r(\bar{x}_a, W, \hat{C}_{l_1}, \hat{C}_{l_2}) \tag{4.3.1}$$

$$\textit{such that} \quad g_a(\bar{x}_a^o, \bar{x}_s^o) + \sum_{j=1}^{n_{dv}} \frac{\partial g_a}{\partial x_j}(x_j - x_j^o) \geq 0 \tag{4.3.2a}$$

$$\textit{and} \quad g_s(\bar{x}_a^o, \bar{x}_s^o) + \sum_{j=1}^{n_{dv}} \frac{\partial g_s}{\partial x_j}(x_j - x_j^o) \geq 0 \tag{4.3.2b}$$

where n_{dv} is the number of design variables and $\hat{C}_{l_1}$ and $\hat{C}_{l_2}$ are the vector lift distributions including structural deflections in the climb and turn respectively and are given by

$$\hat{C}_{l_i} = \hat{C}_{l_i}(\bar{x}_a^o, \bar{x}_s^o) + \sum_{j=1}^{n_{dv}} \frac{\partial \hat{C}_{l_i}}{\partial x_j}(x_j - x_j^o) \qquad i = 1,2 \tag{4.3.3}$$

The upper and lower bounds on the design variables are given as

$$(1 - \lambda_j)x_j \leq x_j \leq (1 + \lambda_j)x_j \tag{4.3.4}$$

where λ_j represents the move limit for the jth design variable. Absolute upper and lower bounds such as those in Eq(4.2.3a) and Eq(4.2.3b) are also applied.

4.4 Approximate Design Analysis

Three design conditions are considered in each design analysis; the turning maneuver, the cruise, and the 5.9g pull-up maneuver. In order to differentiate between these conditions we use a subscript i , where i can have the values 1,2, or 3 corresponding to the turn, cruise, and pull-up maneuvers respectively.

The approximate design analysis proceeds in the following manner. First, the geometry of the wing is established using the given design variables. Next, the base rigid-wing lift distribution, $\bar{C}_{l_b}^o$, is determined for the initial wing using a VLM analysis, and the initial A matrix, A^o, is calculated using either exact

or approximate methods as described in Sections 3.2 and 3.3. By systematically perturbing each of the 4 planform geometry variables and the 2 twist variables (these are the only variables that effect the base rigid-wing lift distribution and A matrix, and correspond to design variables 4-9) and performing repeated VLM and A matrix calculations, we obtain the aerodynamic sensitivities $\frac{\partial \bar{C}_{l_b}}{\partial x_j}$ and $\frac{\partial A}{\partial x_j}$. A linear approximation to the rigid-wing base lift distribution and A matrix may now be constructed as

$$\bar{C}_{l_b} = \bar{C}^o_{l_b} + \sum_{j=4}^{9} \frac{\partial \bar{C}_{l_b}}{\partial x_j}(x_j - x_j^o) \tag{4.4.1}$$

$$A = A^o + \sum_{j=4}^{9} \frac{\partial A}{\partial x_j}(x_j - x_j^o) \tag{4.4.2}$$

(Although the A matrix does depend on the angle of attack, it was found that the derivative of A with respect to the incidence angle was at least an order of magnitude smaller than the largest of the other derivatives of A and therefore was neglected.) At this point, the total weight of the wing, based on the initial design variables is determined by the structural analysis code. The subsequent steps are separated into three groups which correspond to the three design conditions, where i= 1,2, and 3.

For the turning maneuver (i = 1), we first determine the vector lift distribution for a rigid wing using Eq(3.1.1) with $\alpha' = \alpha'_1$, corresponding to the turn, and $\bar{\delta} = 0$. The total lift coefficient, C_{L_1} is then determined from the section lift

coefficients as described in section 2.3. Since the total lift coefficient remains the same after the structural deflections have been taken into account (only its spanwise distribution changes), it may be used to determine the load factor in the turn, n_1 , as in Strauch [1]. The velocity in the turn and dynamic pressure, q_1 are also determined. An exact aeroelastic analysis is now performed to find $\hat{C}_{l_1}$, the vector lift distribution including structural deformations. Once the section lift distribution is obtained, the induced drag coefficient may be calculated using the method described in Section 2.4, and the total drag coefficient in the turn including profile drag is determined. The climb speed in the turn may now be calculated using Eq(2.1.1) and Eq(2.1.2), and the aerodynamic constraints are evaluated.

This procedure is used to determine initial values for the vector lift distribution, $\hat{C}^o_{l_1}$, and aerodynamic constraints, g^o_a. By repeating the above process n_{dv} times, while perturbing one design variable at a time, we obtain the sensitivities of the vector lift distribution and aerodynamic constraints with respect to each design variable, $\frac{\partial C_{l_1}}{\partial x_j}$ and $\frac{\partial g_a}{\partial x_j}$. It is noted that when design variables 4-9 are perturbed, a new base lift distribution $\overline{C}_{l_b}$ and A matrix must be obtained from Eq(4.4.1) and Eq(4.4.2). We may now construct a linear approximation for the vector lift in the turn and aerodynamic constraints as given in Eq(4.3.3) and Eq(4.3.2a).

In a similar manner, for the turn ($i=2$), the rigid wing lift distribution is determined using Eq(3.1.1) with $\alpha' = \alpha'_2$, corresponding to the cruise

maneuver, and $\bar{\delta} = 0$. It is noted that the load factor during cruise n_2 is equal to 1. The total lift coefficient, C_{L_2}, is obtained using the rigid wing lift distribution and the method in section 2.3. The cruise velocity is determined from Eq(2.1.3) and the dynamic pressure in cruise q_2 is calculated. An exact aeroelastic analysis is now performed to determine the vector lift distribution including aeroelastic effects $\hat{C}_{l_2}$.

This procedure is used to calculate $\hat{C}^o_{l_2}$ and repeated while systematically perturbing each design variable to obtain the sensitivities $\frac{\partial \hat{C}_{l_2}}{\partial x_j}$. A linear approximation for $\hat{C}_{l_2}$ may now be constructed as given in Eq(4.3.3).

The final condition is the 5.9g, 43 m/s pull-up maneuver (i=3) where the structural constraints are imposed. This point came from the V-n diagram for a similar glider. Given the load factor and the velocity, we can determine the lift coefficient C_{L_3} for the pull-up manuever. From this and the assumption of a linear lift-curve slope we obtain α_3, the angle of attack in the pull-up. We now determine the dynamic pressure q_3 and perform an exact aeroelastic analysis to obtain the twist vector $\bar{\delta}_3$ and the load vector $\bar{F}_3$. The structural constraints, including the strains in the spar caps and skin and the shear stresses in the spar webs, are now evaluated. Finally we solve the eigenvalue problem, Eq (2.7.9), for the divergence dynamic pressure, q_d, and evaluate the dynamic pressure constraint.

Again, this procedure is used to determine g_s^o and the sensitivities $\frac{\partial g_s}{\partial x_j}$ allowing the construction of the linear approximation to the structural constraints as given in Eq(4.3.2b).

Once these linear approximations have been determined, we may proceed with the approximate optimization process as discussed in the previous section. The objective function, Eq(2.1.12), may be determined from the approximate lift distributions and their corresponding drag coefficients using Eqs (2.1.1)-(2.1.4). A schematic for the design process is given in Fig. 12.

Chapter 5. Discussion of Results

Past research has focused on clearly establishing the advantages of the integrated design procedure over the more traditional sequential/iterated approach. In the investigations reported in Refs. [1] and [2], a series of design studies was performed for a sailplane wing in order to evaluate differences in the integrated and iterative, sequential design processes. The thermal strength was an input parameter and the results were found to be highly sensitive to this strength. Because sailplanes depend on their weight for speed during cruise, they often carry ballast to increase their cross-country speed. This is done when the thermal strength is strong enough that the loss in climb speed due to the extra weight is compensated by the gain in cruise speed. However, in normal aircraft design, minimum weight is usually desirable for maximum performance. To ensure that the integrated design process would minimize weight to obtain the maximum cross-country speed, an extremely weak Horstmann thermal profile was chosen. For this thermal,

the air velocity decreases linearly with increasing radius, and is 0.9 $\frac{m}{s}$ at the thermal center. A sketch of this profile is shown in Fig. 13.

Also, for the original study, both the iterative sequential and integrated design processes were started from a design corresponding to an existing sailplane that was designed and built at Rensselear Polytechnic Institute, the RP-2. Specifications for this sailplane are shown in Fig. 14. It is also noted that the RP-2 was not fully optimized and its design was not based on the same very weak thermal profile. In the first series of designs, the wing span was set at 13.5 meters, as in the RP-2 design. Three designs were generated. A sequential, iterative design, an integrated design maximizing cross-country speed, and an integrated design minimizing weight subject to a minimum cross-country speed requirement equal to that obtained by the iterative design. The results are shown in Table 6. The increase in performance of the integrated design as compared to the iterative design was 1.0 percent, with a 4 percent reduction in weight. The integrated minimum weight design had a weight 11 percent lower than that of the iterative design with the same cross-country speed.

The large effect on weight of the integrated design as compared to the small effect on performance is due to an imbalance between the two interactions in the structural and aerodynamic design. The first interaction allows changing aerodynamic load distributions to reduce stresses. The design variables employed in this study allowed substantial freedom to benefit from this

interaction to reduce structural weight. The second interaction is taking advantage of structural deformations to improve performance. This effect is very weak in the present problem because of the relatively low g at the climb phase and because the composite skins were not utilized to obtain strong bending-torsion coupling.

The results in Table 6 indicate a trend where a larger portion of the lift is moved inboard as the weight becomes lower. This is acheived by manipulating the twist angles at the break and tip, by reducing the chord at the tip, and by reducing the distance to the break. In addition, as the weight decreases, the wing also becomes more flexible.

In the original design study, the costs associated with constraint and objective function evaluation were small and the analysis codes could be connected directly to the optimization algorithm. The practicality of the approach and the computational efficiency were not considered. In the present study, the sailplane design problem is analyzed using 8 spanwise sections and 80 vortex panels. Ninety structural nodes and 409 structural elements are used in the finite element model. An attempt to perform a design study without using the cost-reducing procedures previously discussed proved unfeasible. The computational requirements for the exact analysis were estimated to be at least 10 hours of IBM 3090 CPU time. However, with the cost-reducing procedures for obtaining efficient cross sensitivities and approximate

optimization procedures, these computational times were significantly reduced.

As in the previous study, the approximate design process was started from a design corresponding to the RP-2 and the wing span was fixed at 13.5 meters.

The complete design process required 4 design cycles ,(as shown in Fig. 12), before convergence was achieved. Convergence was determined when the optimization code, NEWSUMT-A, ceased to reduce the objective function below that of the previous cycle. Each design cycle required approximately 176 CPU seconds on the IBM 3090, giving a total of 704 CPU seconds for the entire design. Approximately 18 percent of the CPU time was needed to calculate the A matrix sensitivities, 52 percent was used to determine the lift and constraint sensitivities and 30 percent of the CPU time was needed for the optimization itself. The convergence history for the design is shown in Fig. 15.

For the present study, the major reduction in computational time results from the approximate optimization procedures and not from the perturbation method. This is due to the fact that only 80 vortex panels were used. In a more realistic aerodynamic analyses many more panels are necessary to obtain an accurate representation of the wing. As shown in Table 3, for the 80 panel case, there is a savings of only 1.2 CPU seconds for the development of the perturbation method compared to the exact method. For the present study, the A matrix is calulated 7 times per design cycle, giving a total savings

of 33.6 seconds for the total design process. For the more realistic 200 panel case, the perturbation method saves 60.4 CPU seconds per A matrix calculation, yielding a savings of 1691.2 CPU seconds for the entire design (based on 4 cycles).

The results for the present integrated design and a sequential/iterative design, using the same analysis methods, are shown in Table 7. In comparing the two designs, the general trends trends are similar to those seen in Table 6. The increase in performance of the integrated design as compared to the iterative design was 1.0 percent, with a 7.0 percent reduction in weight. Also, as in Table 6, a larger portion of the lift is moved inboard as the weight decreases. This is again achieved by reducing distance to the break, by reducing the chord at the tip, and by manipulating the geometric twist distribution. Differences in these results as compared to those of Table 6 can be attributed to the differences in analysis methods.

Chapter 6. Conclusions

In previous work, Ref. [2], our investigation of the design process of a composite sailplane wing clearly demonstrates the superiority of an integrated design approach over an iterative, sequential procedure. Within the assumptions of very rudimentary aerodynamic and structural analyses, the integrated optimization procedure yielded superior designs. The integrated procedure was able to capitalize on favorable interactions between the aerodynamics and the structure. These interactions included distributing structural material so the deformations did not reduce aerodynamic performance, and reducing the weight of the wing to increase the overall performance. Wing structural weight was reduced by concentrating more of the lift inboard and by reducing the planform area of the wing, resulting in lower root bending moments. The reduced weight was accompanied by reduced torsional stiffness and greater deformations. But this did not depreciate the aerodynamic performance because the added deformations

were compensated for by adding twist and distributing the structural material prudently. The separation of the two disciplines in the iterative procedure did not allow such interactions to be taken into account and applied towards improvement of the design.

Along the lines of a more complete integrated design process, we have replaced the rudimentary analysis tools of the lifting-line theory and a simple beam model of the wing structure with a more realistic vortex-lattice method and and a finite-element analysis of the wing structure. These methods provide a more exact analysis and allow more general wing shapes, however, they introduce the need for more independent design variables and constraints and are significantly more expensive than the methods used in the previous study.

These more realistic analysis methods have been used in the present design study, where we consider the same structural/aerodynamic design of a sailplane wing to investigate the computational costs of the multidiscipinary design optimization process. An attempt to perform a design study without using the cost-reducing procedures proved unfeasible and was estimated to require at least 10 hours of IBM 3090 CPU time. We have considered two methods for reducing the computational burden: (i) development of efficient methods for cross-sensitivity calculation using perturbation mathods; and (ii) the use of approximate numerical optimization procedures. The incorporation of these methods has reduced the CPU time from an estimated 10 hours, to

approximately 12 minutes, for the entire design process. The results for the present designs have the same general trends as those found in past studies.

Although we have made a step in the general direction of a more realistic design problem, we are still far what is necessary to obtain a credible design. A more complete design process should include design variables for the wing thickness at each station, and would require a boundary layer analysis to account for skin-friction and form drag. A more complex aeroelastic analysis, including the effects of change in moment due to torsional deformations and the effects of vertical displacements should be incorporated. Also, the present aerodynamic analysis is valid only for low speed flight, where the governing equations are linear, and finite differences may be used to evaluate the cross-sensitivities.

There appears to be an enormous potential for design improvement utilizing integrated design procedures. Improved designs may be obtained not only through aerodynamic/structural interactions, as discussed here, but also through integration procedures which would include the control and propulsion systems. However, before this process can be made feasible, significant reductions to the computational burden, such as those initiated here, must be developed. These efficient design methods, along with forecasted significant performance gains in computers, will make integrated design procedures a future reality.

List of References.

1. Strauch, G.J., *Integrated Multidisciplinary Design of a Sailplane Wing* , Thesis VPI&SU, 1985.

2. Grossman B., Strauch, G.J., Eppard, W.M., Gurdal, Z., and Haftka, R.T., "Integrated Aerodynamic/Structural Design of a Sailplane Wing ," *AIAA Paper* , AIAA-86-2623.

3. Helwig, Gunter, *Wing Shape Optimization for Maximum Cross-Country Speed with Mathematical Programming* , Renssalaer Polytechnic Institute, N79-23899, 1979.

4. Bertin, J.J. and Smith, M.L., *Aerodynamics for Engineers* , Prentice Hall Inc., 1979.

5. Multhopp, H., " Method for Calculating the Lift Distribution of Wings (Subsonic Lifting Surface Theory)," *Reports and Memoranda 2884* , Aeronautical Research Council, Jan 1950.

6. Kalman, J.P., Giesing, J.P., and Rodden, W.P., " Spanwise Distribution of Induced Drag in Subsonic Flow by the Vortex Lattice Method, " *Journal of Aircraft* , Nov.-Dec. 1970, Vol. 7, No. 6, pp 574-576.

7. Haftka, R.T. and Starnes, J. H. Jr., *WIDOWAC: Wing Design Optimization with Aeroelastic Constraints - Program Manuel* , NASA TM X-3071, 1974.

8. Miura, Hirokazy and Lucien A. Schmit, Jr., *NEWSUMT - A Fortran Program for Inequality Constrained Function Minimization - Users Guide* , University of California, Los Angeles.

9. Thereja, Rajiv and Haftka, R.T., *NEWSUMT-A A Modified Version of NEWSUMT for Inequality and Equality Constraints* , VPI&SU, March 1985.

10. Schmit, L. A. and Farshi, B., " Some Approximation Concepts for Strutural Synthesis, " *AIII J.* Vol. 12, No. 5, 1974, pp. 692-699.

TABLE 1.

CPU Times for A Matrix - Exact

	80 panels	120 panels
Base solution	0.87 sec	2.15 sec
Calculate V	0.64 sec	1.44 sec
Solve system	1.76 sec	8.82 sec
Convert Γ to C_l	2.48 sec	8.28 sec
Total	5.75 sec	20.69 sec

TABLE 2.

CPU Times for A Matrix - Perturbation

	80 panels	120 panels
Base solution	0.87 sec	2.15 sec
Calculate RHS	1.04 sec	2.52 sec
Solve system	0.17 sec	0.68 sec
Convert Γ to C_l	2.48 sec	8.28 sec
Total	4.56 sec	13.63 sec

TABLE 3.

Summary of CPU times for A matrix

Panels	Exact CPU sec	Perturb CPU sec	Percent savings
80	5.8	4.6	20.7
120	20.7	13.6	34.3
160	54.3	30.3	44.2
200	116.8	56.4	51.7

TABLE 4.

Design Variables

3 Performance Design Variables	1. Angle of attack during turn
	2. Angle of attack during cruise
	3. Radius of turn
6 Geometric Design Variables	4. Twist angle at the break relative to the root
	5. Twist angle at the tip relative to the root
	6. Chord length at the root
	7. Chord length at the break
	8. Chord length at the tip
	9. Distance to the break
32 Structural Design Variables	10-17. Spar cap thickness for each wing section
	18-25. Spar web thickness for each wing section
	26-41. Skin thickness for each wing section

TABLE 5.

Design Constraints

3 Stall Constraints During Turn	1. No stall at root
	2. No stall at the break
	3. No stall at tip
3 Performance Constraints	4. Bank angle less than 50 deg
	5. Climb speed greater than zero
	6. Minimum divergence speed
81 Structural Constraints (43 m/s, 5.9g)	7-14. Maximum spar cap strain for each wing section (.3 percent)
	15-22. Maximum shear stress for each wing section, web shear less than 6000 $\frac{N}{cm^2}$
	23-86. Wing skin must satisfy Tsai-Hill strength constraint for each wing section

TABLE 6.

Previous Design Results (0.9 m/s thermal)

	Iterated Sequential	Integrated Design	Weight Minimization
Cross-Country Speed (m/s)	3.44	3.48	3.44
Mass of One Wing (Kg)	13.0	12.5	11.6
Chord Lengths			
Root	100	105	105
Break (cm)	100	98	98
Tip	41	38	36
Distance to Break (cm)	315	249	245
Twist (deg)			
Break	0.23	0.16	0.15
Tip	-0.22	-0.32	-0.01
Aspect Ratio	15.9	16.5	16.8
Wing Area (m^2)	11.5	11.1	11.0

TABLE 7.

Present Design Results (0.9 m/s thermal)

	Iterated Sequential	Integrated Design
Cross-Country Speed (m/s)	2.80	2.83
Mass of One Wing (Kg)	16.6	15.43
Chord Lengths		
Root	110	108
Break (cm)	110	105
Tip	45	44
Distance to Break (cm)	313	285
Twist (deg)		
Break	0.94	1.27
Tip	-0.01	0.74
Aspect Ratio	14.3	15.1
Wing Area (m^2)	12.7	12.1

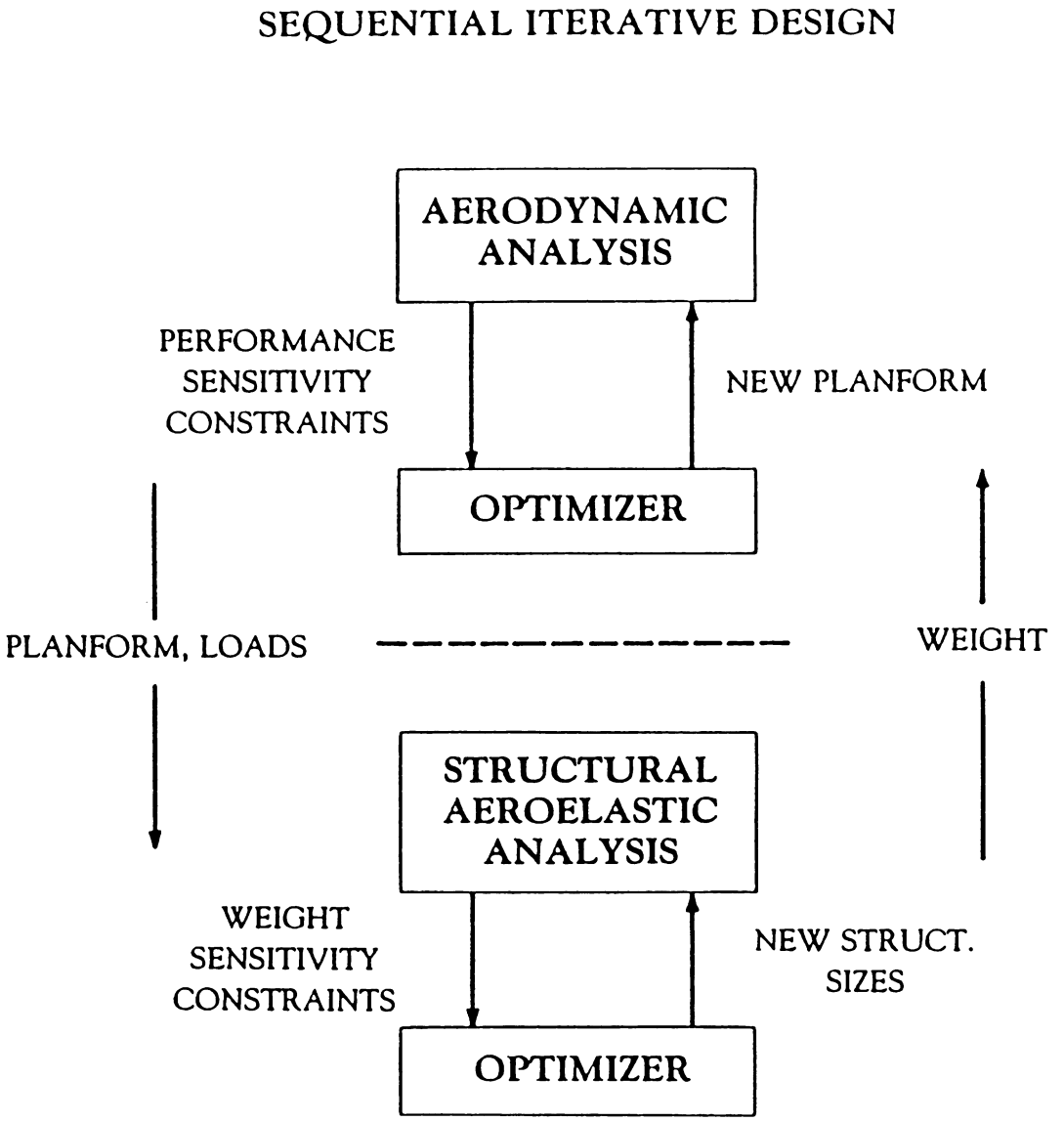

Figure 1. Schematic of Iterative Sequential Design Procedure

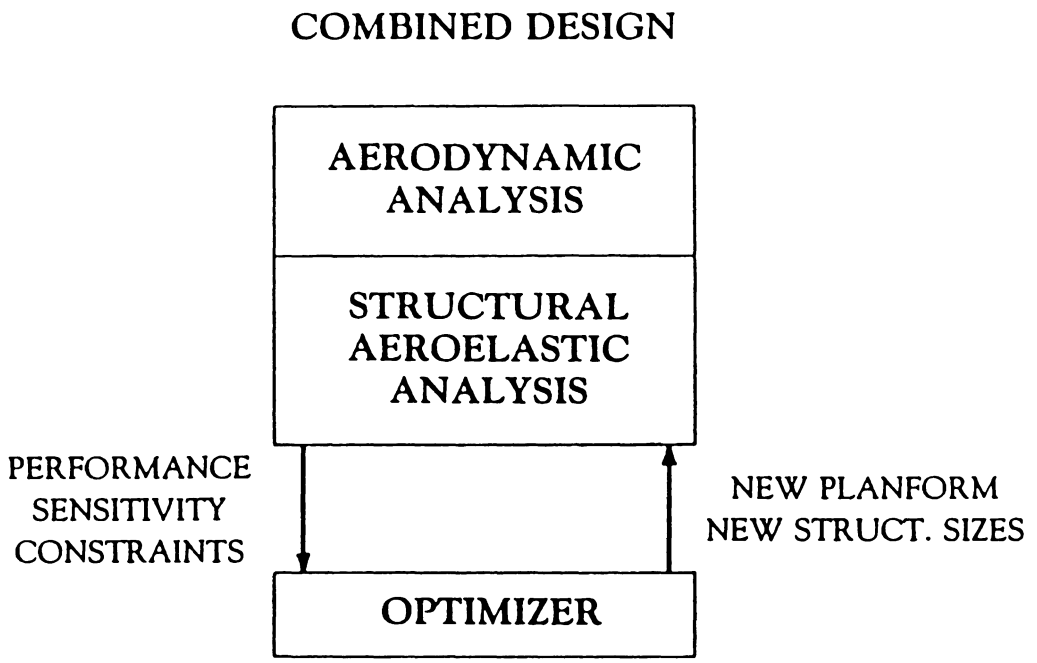

Figure 2. Schematic of Integrated Design Procedure

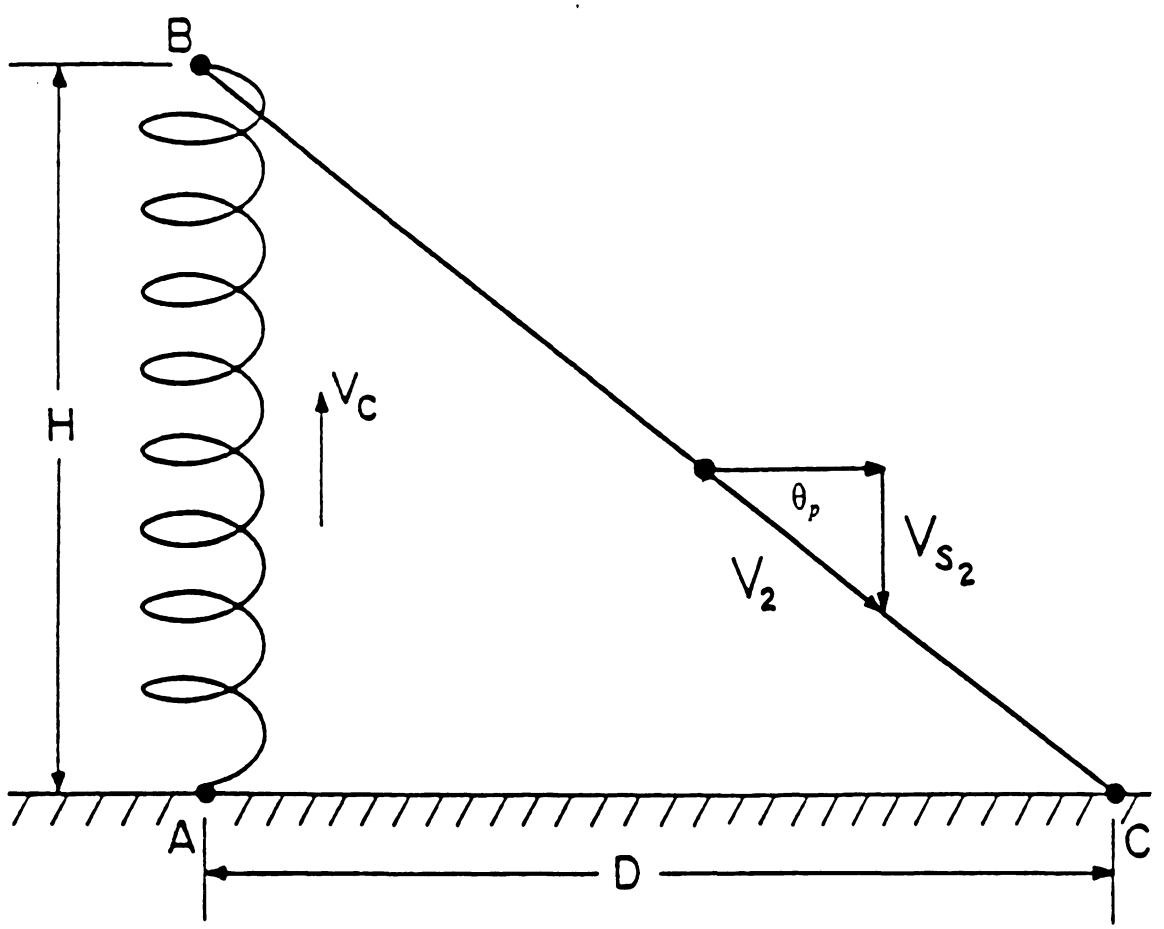

Figure 3. Sailplane Mission Profile

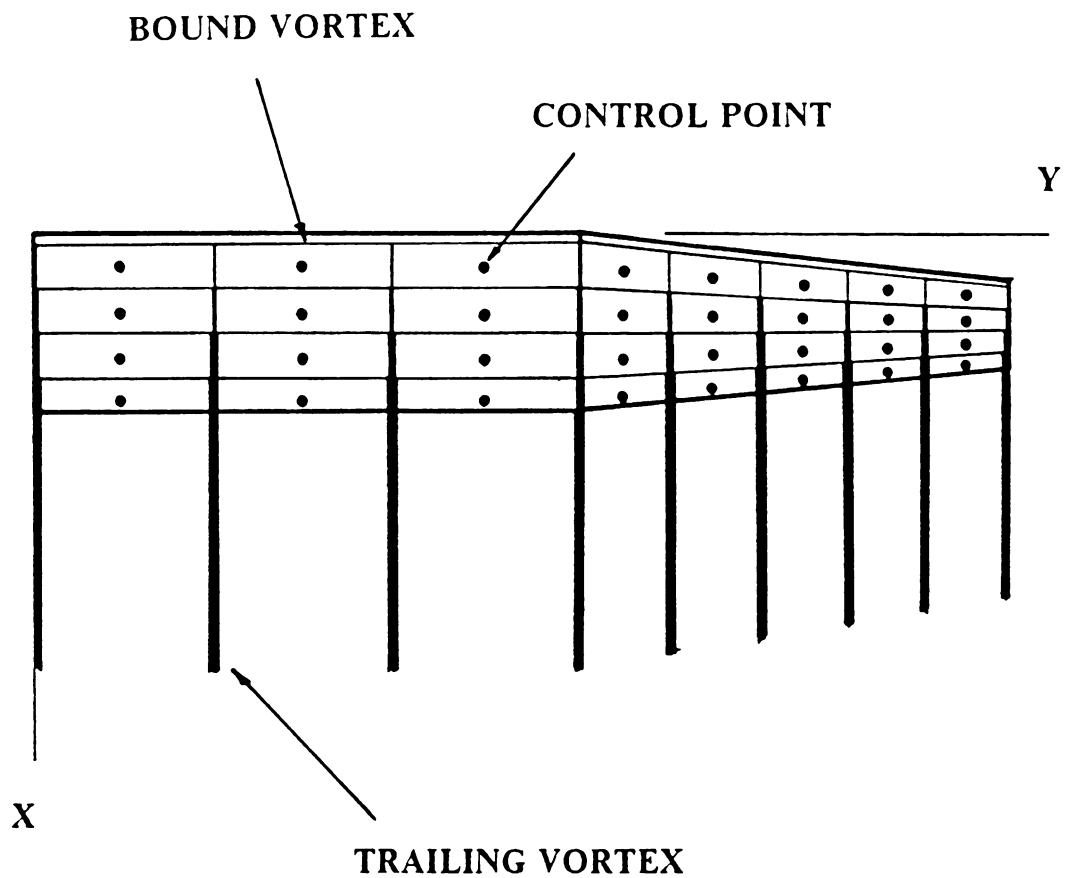

Figure 4. Coordinate System and Horseshoe Vorticies for VLM

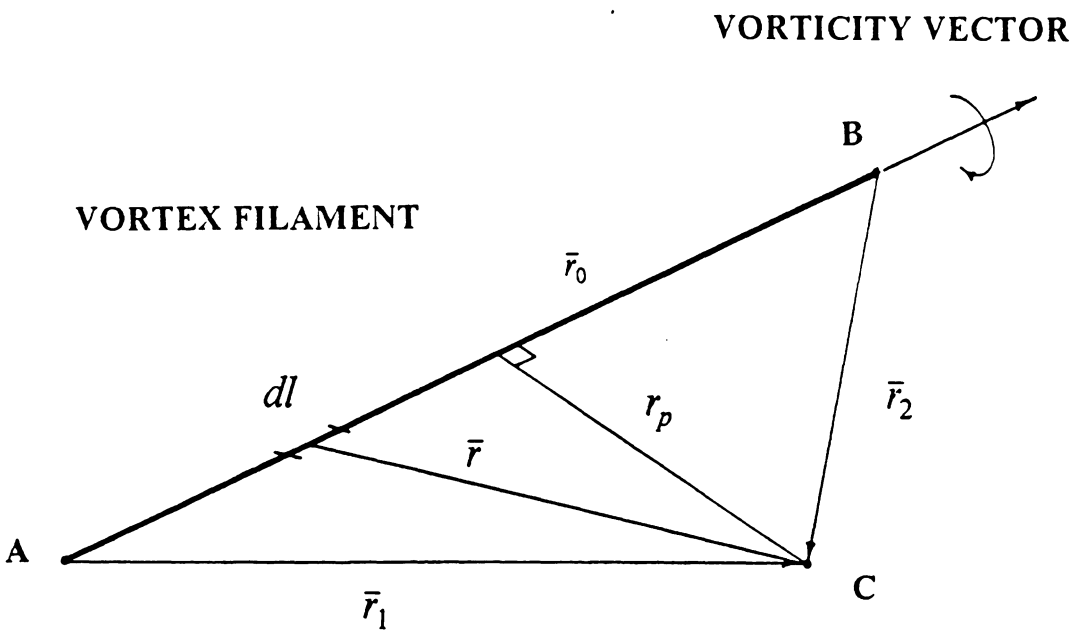

Figure 5. Nomenclature for Finite Length Vortex Segment

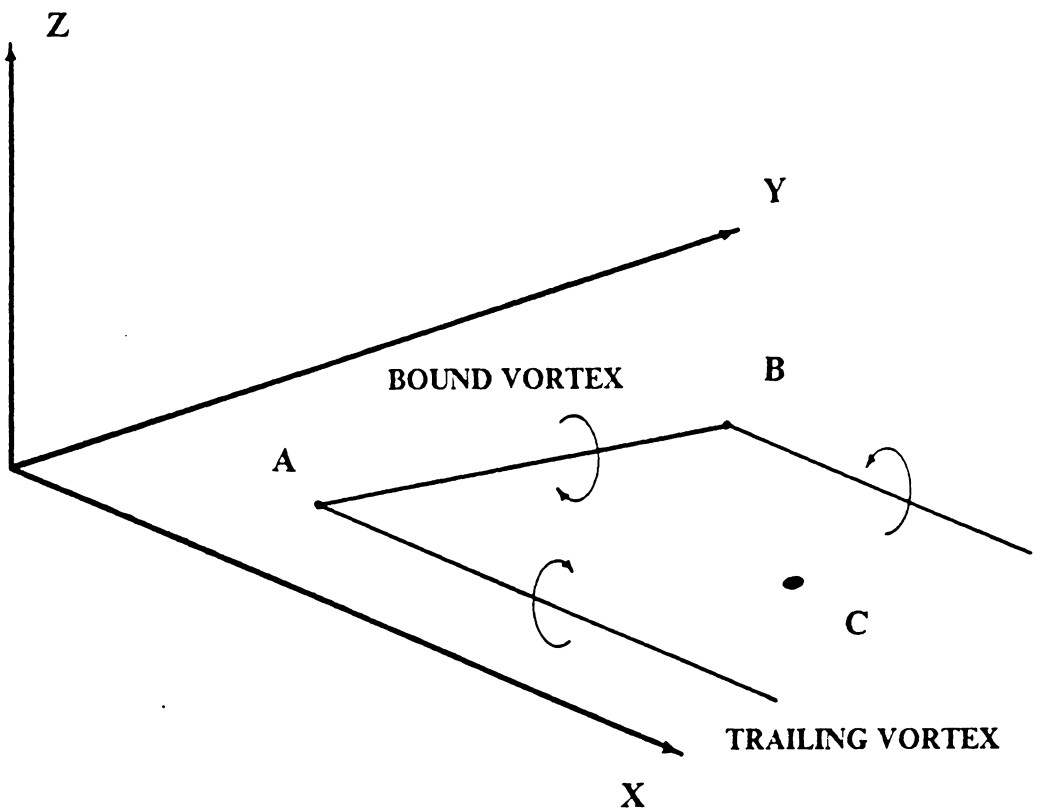

Figure 6. Typical Horseshoe Vortex

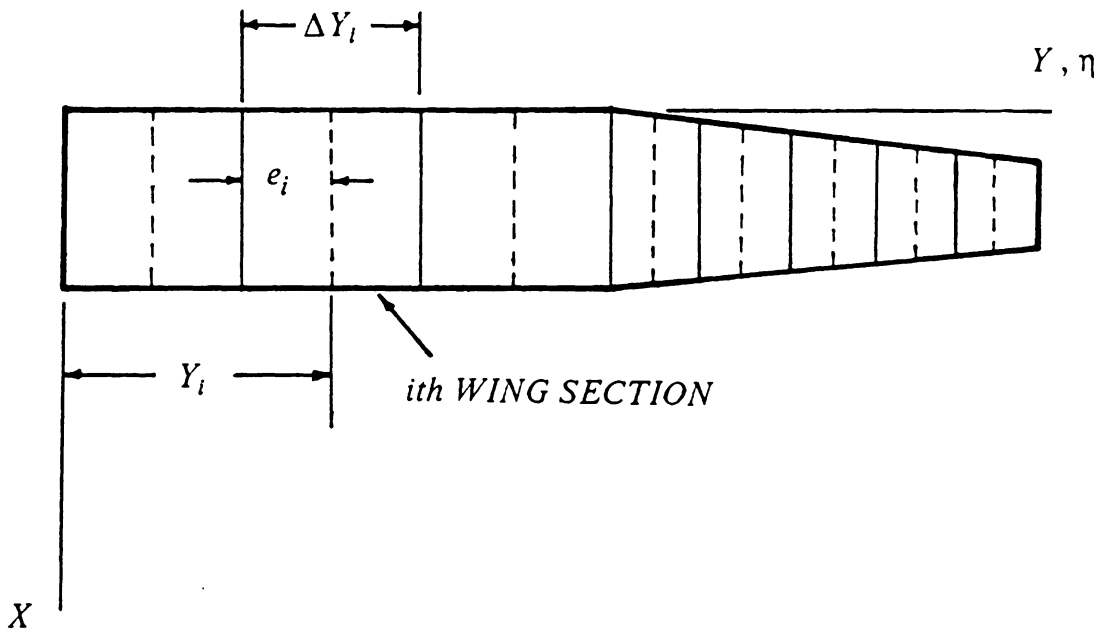

Figure 7. Wing Section Nomenclature

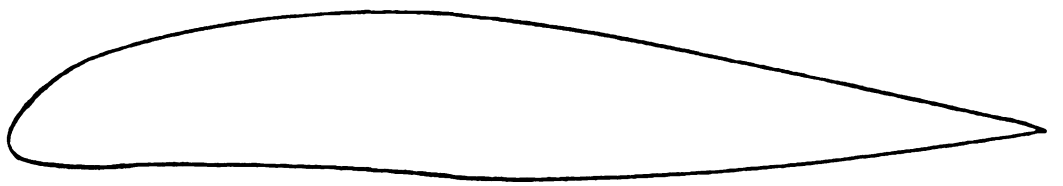

BoAR 80-RPVT-163

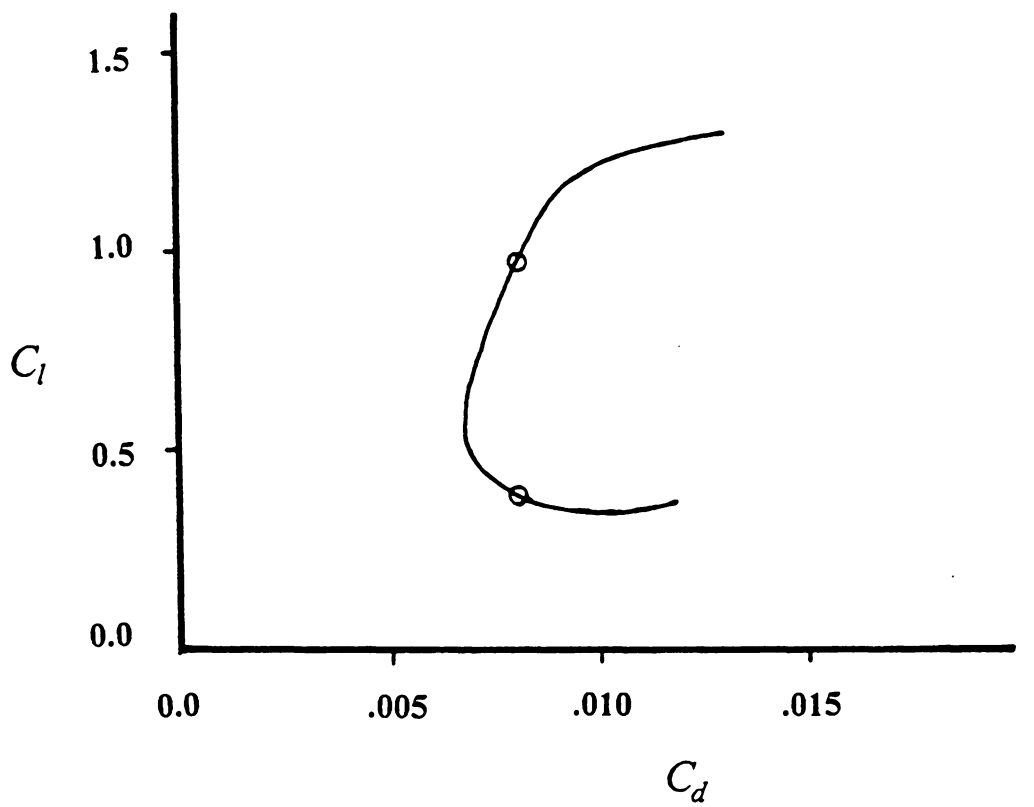

Figure 8. Airfoil shape and Drag Characteristics

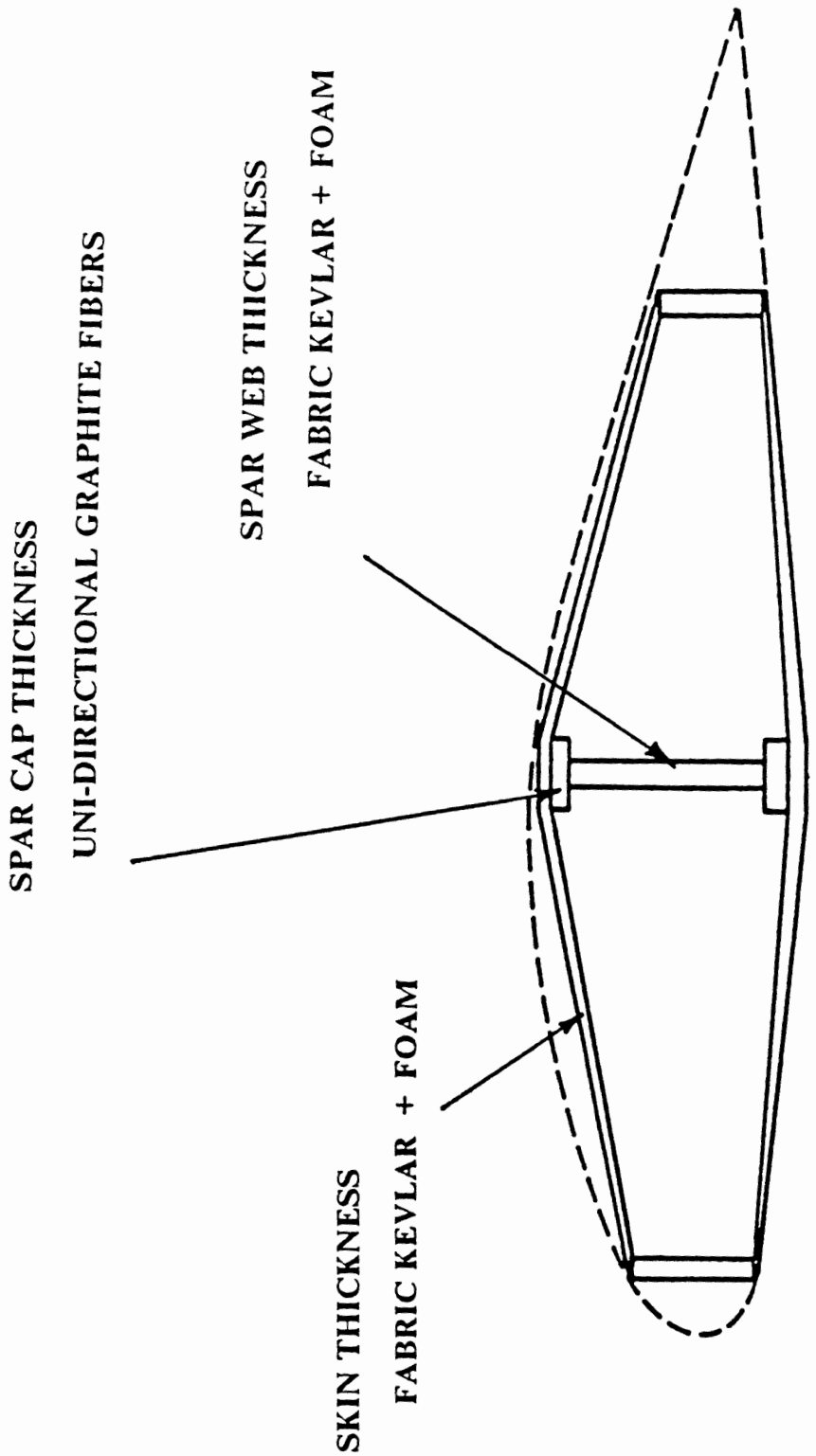

Figure 9. Structural Details of the Wing

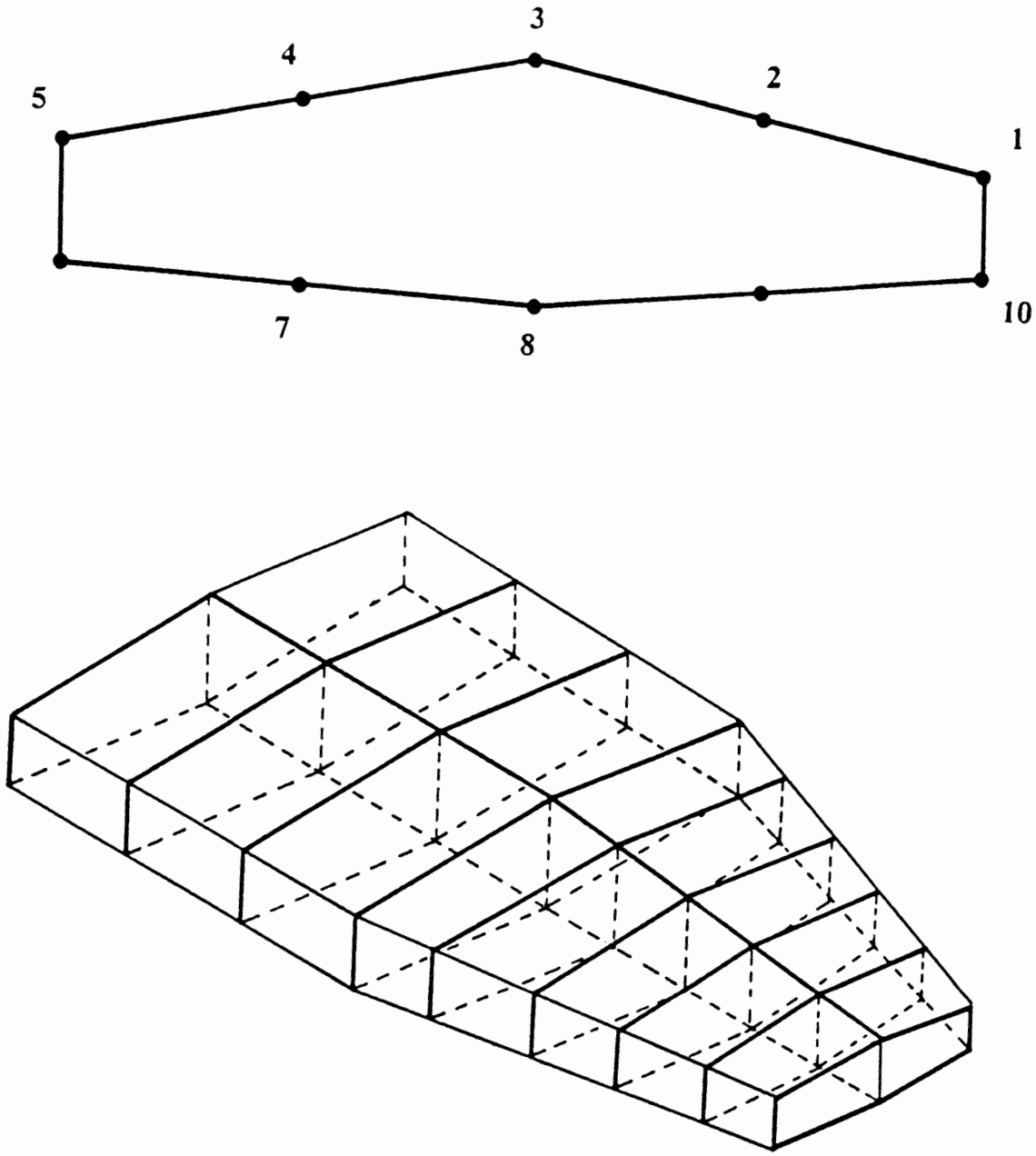

Figure 10. Structural Wing Sections and Nodes

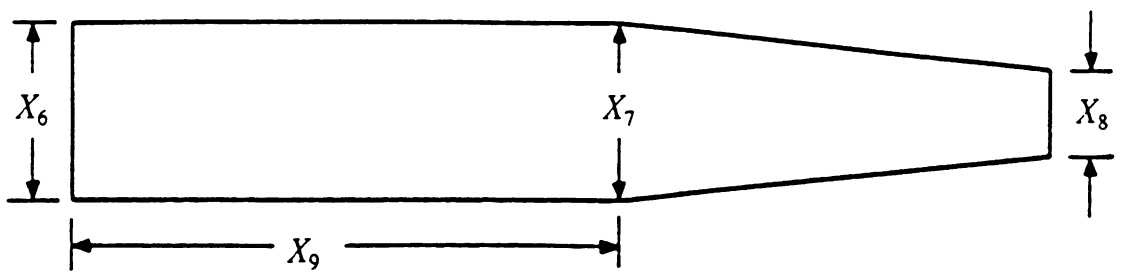

Figure 11. Planform Geometry Variables

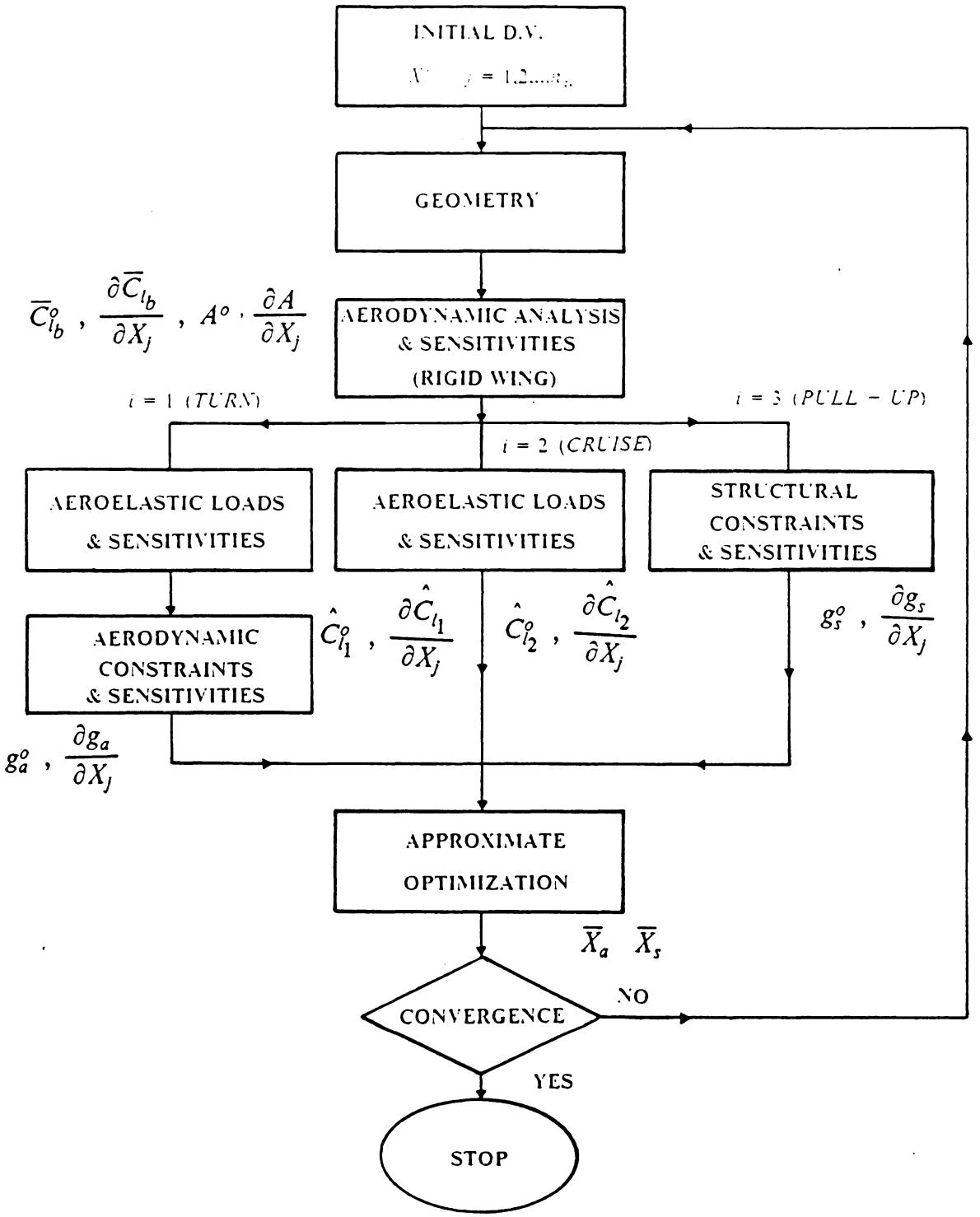

Figure 12. Schematic of Approximate Design Procedure

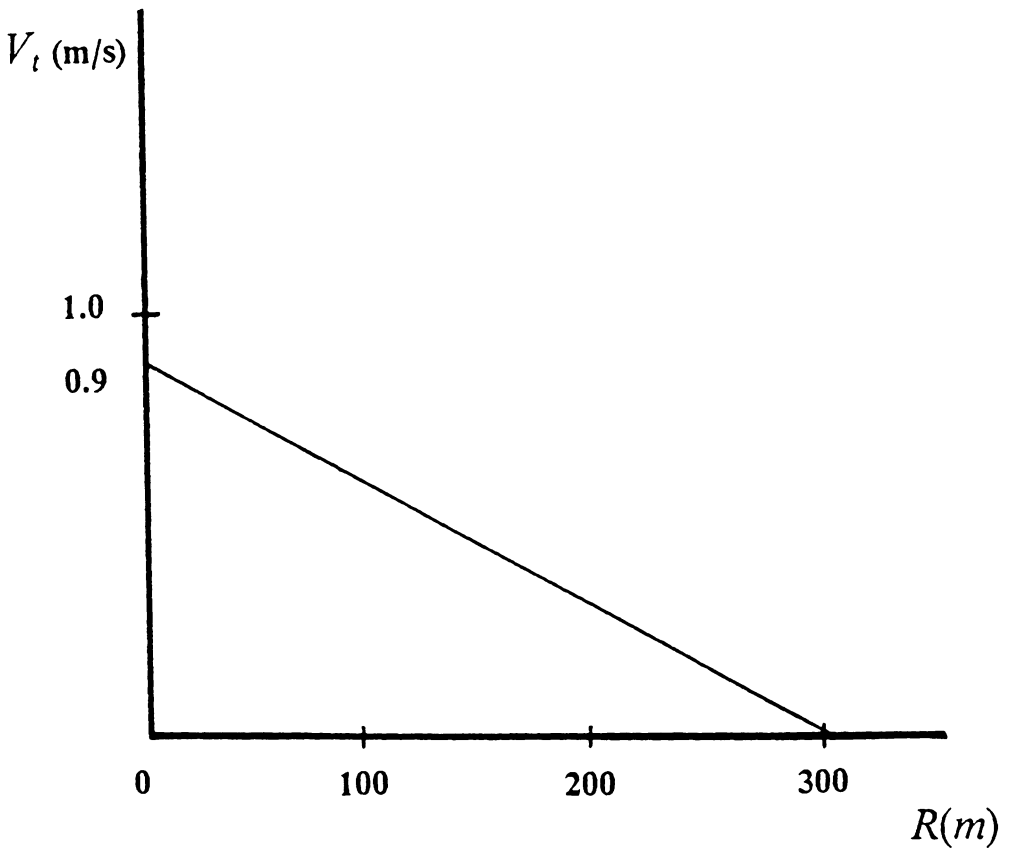

Figure 13. Thermal Profile (0.9 m/s)

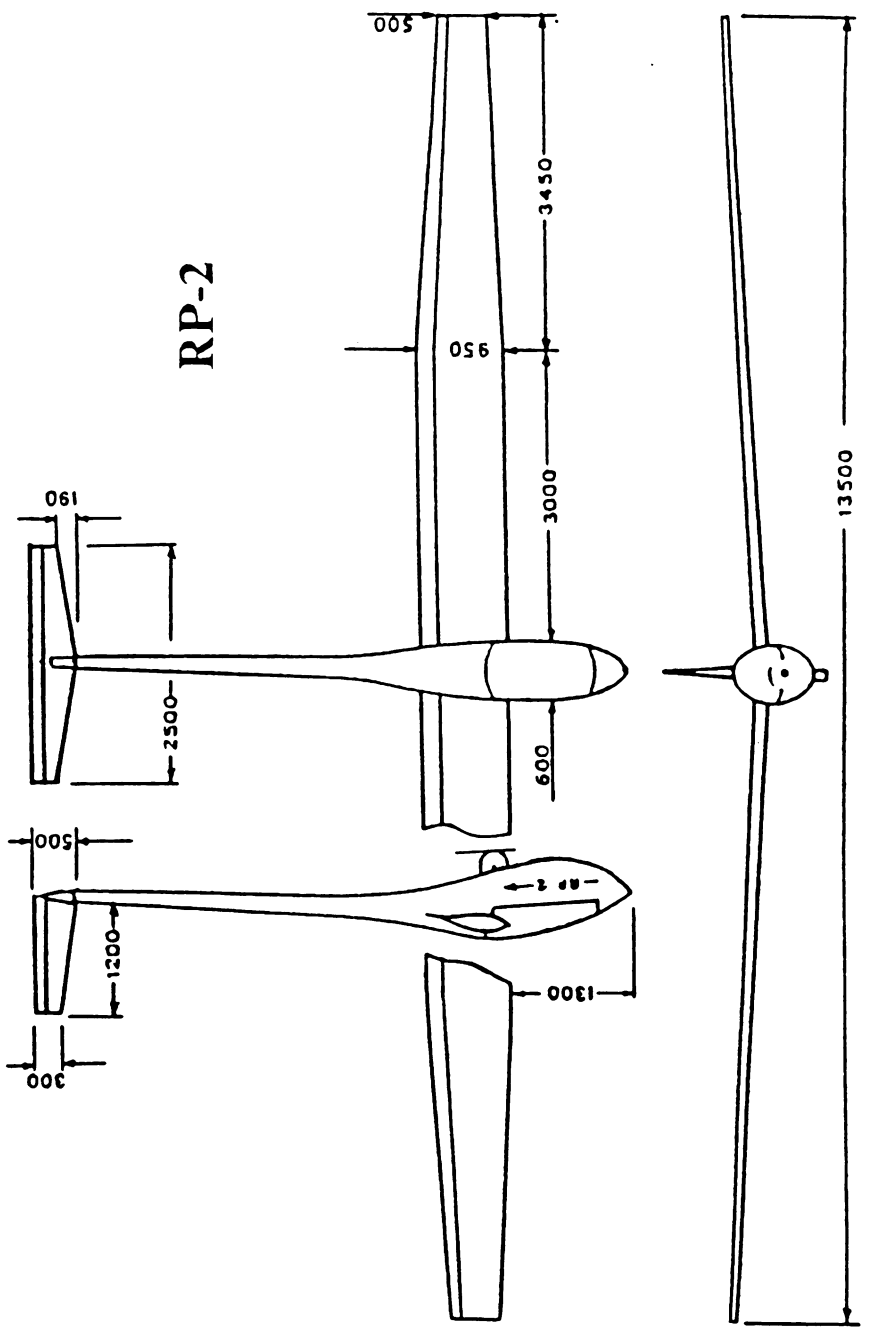

Figure 14. RP-2 Sailplane

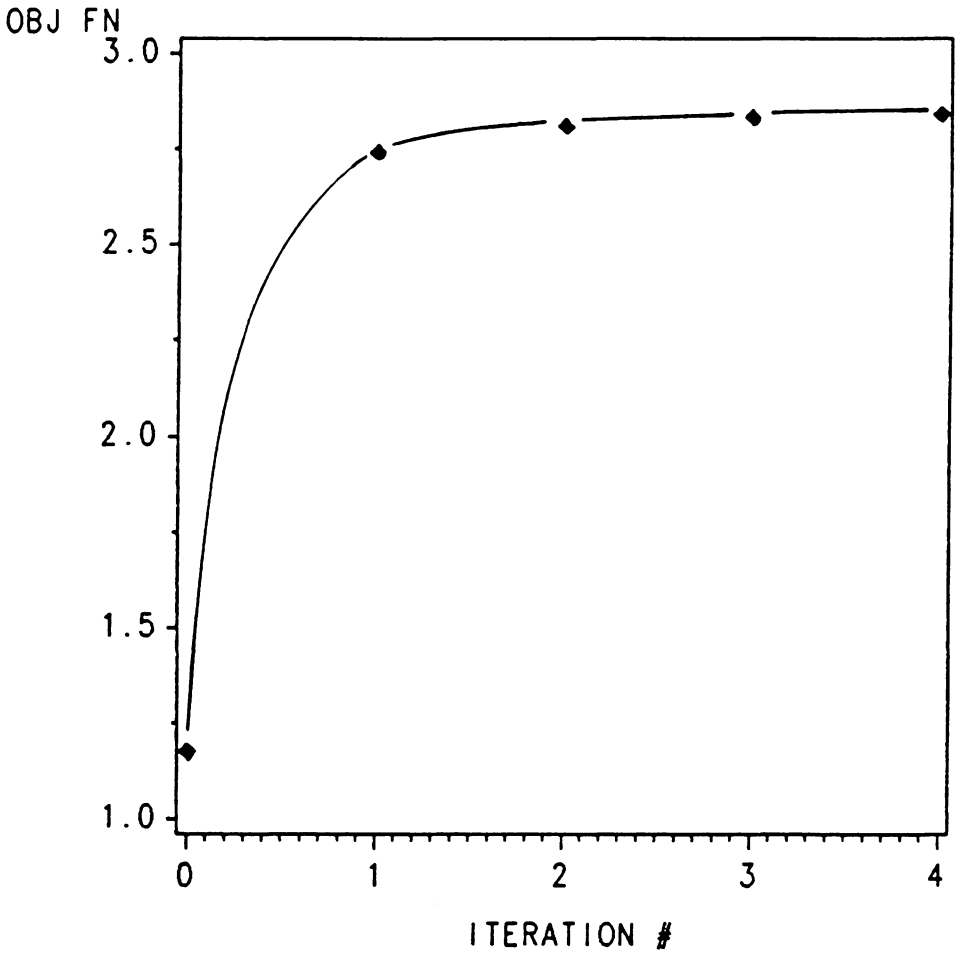

Figure 15. Objective Function vs. Number of Iterations

The vita has been removed from the scanned document